



1 **Constraining the timing and processes of pediment formation and** 2 **dissection: implications for long-term evolution in the Western Cape,** 3 **South Africa**

4 Janet C. Richardson¹, Veerle Vanacker², David M. Hodgson³, Marcus Christl⁴, Andreas Lang⁵

5 ¹Geography and Geology: Department of History, Geography and Social Sciences, Edge Hill University, Ormskirk, L39 4QP,
6 UK

7 ²Earth and Life Institute, Centre for Earth and Climate Research, Université catholique de Louvain, Louvain-la-Neuve,
8 1348, Belgium

9 ³School of Earth and Environment, University of Leeds, Leeds, LS2 9JT, UK

10 ⁴Ion Beam Physics, ETH Zürich, Zürich, Otto-Stern-Weg 5, CH 8093, Switzerland

11 ⁵Department of Geography and Geology, Universität Salzburg, Salzburg, A-5020, Austria

12

13 *Correspondence to:* Janet C. Richardson (Janet.Richardson@edgehill.ac.uk)

14 **Abstract.** Pediment surfaces are a widespread feature of the southern African landscape and have long been regarded as ancient
15 landforms. Cosmogenic nuclide data from four pediment surfaces in the Gouritz catchment, Western Cape, South Africa are
16 reported, including boulder surface samples and a depth profile through a colluvial pediment deposit. The results indicate low
17 surface lowering rates (0.315 to 0.954 m My⁻¹) and minimum exposure ages of 0.678 – 4.462 My (assuming denudation rates
18 of 0.3 m My⁻¹). Duricrusts have developed in the pediments and are preserved in some locations, which represent an internal
19 geomorphic threshold limiting denudation and indicate at least 1 My of geomorphic stability following pediment formation.
20 The pediments and the neighbouring Cape Fold Belt are deeply dissected by small order streams that form up to 280 m deep
21 river valleys in the resistant fold belt bedrock geology, indicating a secondary incision phase of the pediments by these smaller
22 order streams. Using the broader stratigraphic and geomorphic framework, the minimum age of pediment formation is
23 considered to be Miocene. Several pediment surfaces grade above the present trunk valleys of the Gouritz River, which
24 suggests that the trunk rivers are long-lived features that acted as local base levels during pediment formation and later incised
25 pediments to present levels. The geomorphic processes controlling the formation and evolution of the pediments varied over
26 time; with pediments formed by hillslope diffusive processes as shown by the lack of fluvial indicators in the colluvial deposits
27 and later development by fluvial processes with small tributaries dissecting the pediments. Integrating various strands of
28 evidence indicates that the pediments are long-lived features. Caution should be taken when interpreting cosmogenic nuclide
29 ages from pediment surfaces in ancient landscapes, as isotopic steady state conditions can be reached.

30 **1 Introduction**

31



32 Recent advancements in geochronology allow erosion rates and exposure ages of landforms to be established, and to place
33 more precise constraints on landscape evolution. Establishing erosion rates and landform ages is essential for linking the
34 evolution of drainage systems to downstream aggradation processes (e.g. Gallagher and Brown, 1999; Chappell et al., 2006;
35 Tinker et al., 2008a; Wittmann et al., 2009; Sømme et al., 2011; Romans et al., 2016), constraining surface uplift and tectonic
36 processes (e.g., Brook et al., 1995; Burbank et al., 1996; Granger et al., 1997; Jackson et al., 2002; Wittmann et al., 2007;
37 Bellin et al., 2014; Vanacker et al., 2015), and palaeo-climate reconstructions (e.g., Margerison et al., 2005; Dunai et al., 2005;
38 Owen et al., 2005; Willenbring and Blackenburg, 2010). Reconstructing ancient landforms and landscape development is
39 challenging due to fragmented preservation and increasing signal overprinting forming a landscape palimpsest (e.g. Chorley
40 et al., 1984; Bloom, 2002; Bishop, 2007; Jerolmack and Paola, 2010; Richardson et al., 2016). However, ancient landscapes
41 and landforms cover a large portion of the globe (e.g., (1) Australia – e.g., Ollier, 1991, Ollier and Pain, 2000, Twidale, 2007
42 a,b; (2) southern South Africa – e.g., Du Toit, 1954, King 1956a, (3) South America – e.g. King, 1956b, Carignano et al., 1999,
43 Demoulin et al., 2005, Panario et al., 2014, Peulvast and Bétard, 2015; (4) Asia – e.g., Gorelov et al., 1970, Gunnell et al.,
44 2007, Vanacker et al., 2007; and (5) Europe – e.g., Lidmar-Bergström, 1988, Bessin et al., 2015) and offer important insights
45 into long-term Earth surface dynamics and landscape evolution (indicating variation in erosion and deposition). Further,
46 pediments and planation surfaces can offer insights into mantle dynamics as they are characterised by undulations with middle
47 (several tens of kms) to very long wavelengths (several thousands of kms) characteristic of lithospheric and mantle
48 deformations (e.g., Braun et al., 2014; Guillocheau et al. 2018).

49

50 The formation of pediments is contentious and four categories of landscape evolution models (Fig.1) exist that address the
51 evolution of pediments and surrounding mountain belts (Dohrenward and Parsons, 2009) (1) range front retreat where
52 channelised fluvial processes are dominant (e.g., Gilbert, 1877; Paige, 1912; Howard 1942); (2) range front retreat where
53 diffuse hillslope and piedmont processes are dominant (e.g., Lawson, 1915; Rich; 1935; Kesel, 1977; Bourne and Twidale,
54 1998; Dauteuil et al., 2015); (3) range front retreat as a result of fluvial and diffusive erosion processes (e.g., Bryan, 1923;
55 Sharp, 1940); and (4) lowering of the range due to channelised flow, catchment development and fluvial incision (e.g., Lustig,
56 1969; Parsons and Abrahams, 1984). Model type 1 acknowledges the occurrence of diffusive processes and model type 2
57 acknowledges the occurrence of channelised erosion processes, but each model argues these are subsidiary formation processes
58 (Gilbert, 1877; Rich, 1935; Howard, 1942). Model type 3 integrates fluvial and diffusive erosion processes, and their relative
59 importance depends on the geomorphic setting (Bryan, 1923; Sharp, 1940) with dominance of diffusive processes in regions
60 with erosion-resistant bedrock lithologies, ephemeral streams and a low range. Model type 4 is associated with drainage basin
61 development in the range, and does not require parallel retreat of the mountain front to form the pediment surfaces (Lustig,
62 1969; Parsons and Abrahams, 1984).

63



84 Pediments or erosional surfaces have been investigated in South Africa since the 1950's (King, 1953; King 1963; Partridge
85 and Maud, 1987), and have denudation rates that are an order of magnitude lower than those in other landforms within southern
86 Africa (van der Wateren and Dunai, 2001; Bierman et al., 2014; Kounov et al., 2015; Fig. 2). The pediment surfaces were
87 inferred as being early Cenozoic to Jurassic in age by King (1963). Large scale erosional features are also a feature of the
88 wider African continent, and extensive research has been undertaken to understand mantle dynamics associated with plateau
89 formation (e.g., Braun et al., 2014; Dauteuil et al., 2015; Guillocheau et al., 2015; Guillocheau et al., 2018). In this paper, we
90 present new isotopic data from pediment landforms in southern South Africa. The main aim of the paper is to constrain
91 landscape development using in-situ produced ^{10}Be isotopes and to establish denudation rates and landform exposure ages.
92 The objectives of the paper are to: 1) assess the formative process associated with pediment evolution; 2) assess the cosmogenic
93 data within a wider geomorphic and geologic framework in order to test the performance of cosmogenic dating in a geomorphic
94 setting with very low denudation rates; and 3) discuss the implications for the wider landscape development of southern South
95 Africa.

96 **2 Regional Setting**

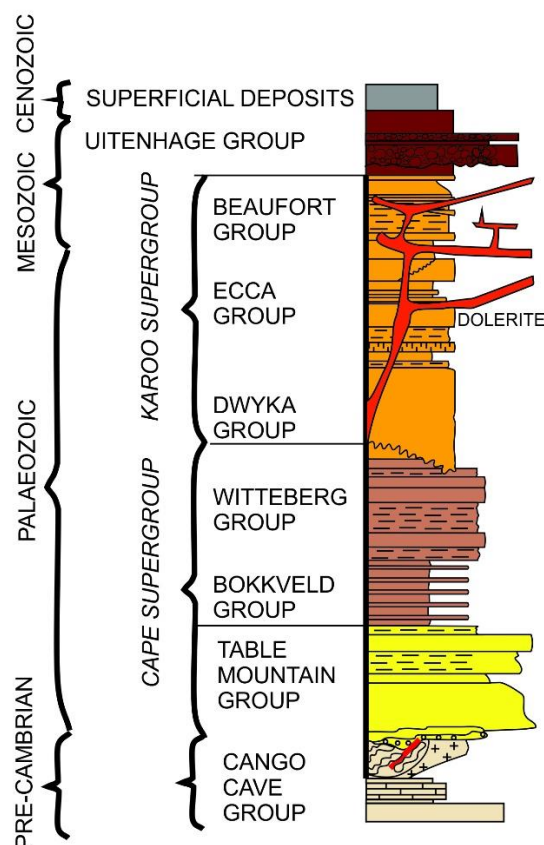
97 **2.1 Geological setting**

98 In the area of study of Western Cape, Southern Africa, the geology is dominated by strata of the Cape and Karoo Supergroups
99 (Fig. 2), which are composed of various sandstone, siltstone and mudstone successions. Both supergroups have been
100 metamorphosed, and the Karoo Supergroup has igneous intrusions. Tectonic shortening of Cape and Karoo Supergroups have
101 resulted in with E-W trending folds that decrease in amplitude northward and form the backbone of the exhumed Cape Fold
102 Belt (CFB)(Paton, 2006; Tinker et al., 2008b; Scharf et al., 2013; Spikings et al., 2015). During the Mesozoic, the rifting of
103 Gondwana initiated large-scale denudation across southern Africa. Using apatite fission track analyses of outcrop and borehole
104 samples, Tinker et al.(2008a) concluded that the southern Cape escarpment and coastal plain underwent 3.3 to 4.5 km of
105 denudation since the mid-late Cretaceous and potentially 1.5 to 4 km within the early Cretaceous, using a thermal gradient of
106 $\sim 20^\circ\text{C}/\text{km}$. Wildman et al. (2015) processed 75 apatite fission track and 8 zircon fission track data from outcrop and boreholes
107 across the southwestern cape of South Africa (from coast to the escarpment). Using a thermal history model of $22^\circ\text{C}/\text{km}$, they
108 obtained an average of 4.5 km of denudation in the Mesozoic. However, the estimates range between 2.2 and 8.8 km of
109 denudation using the upper and lower ranges of the geothermal gradient and possible thermal histories bounded by 95%
110 significance intervals, which provides uncertainty on the inferred model. Richardson et al. (2017) used reconstructed geological
111 cross sections and drainage reconstruction to model up to 4-11 km of denudation.

112

113

114



115

116 **Figure 2: Stratigraphic chart showing the major lithostratigraphic units of South Africa.**

117

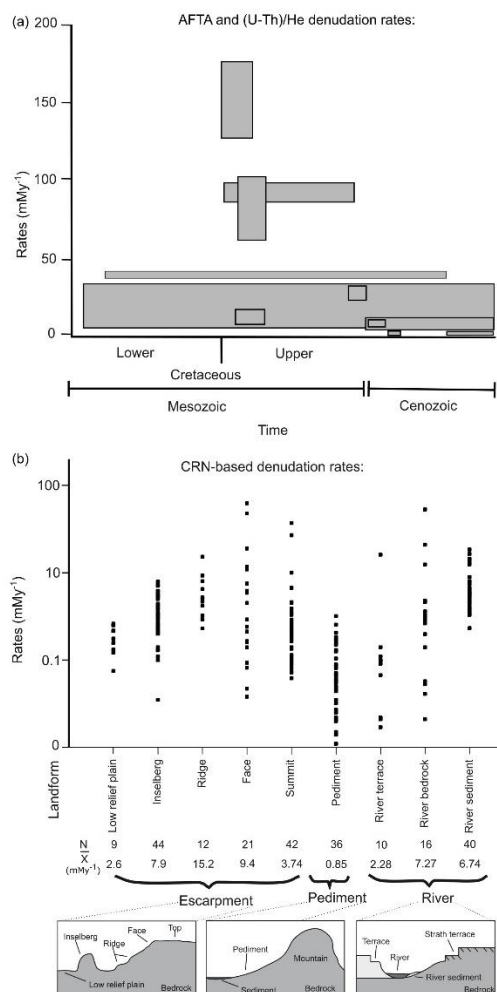
118 The mechanisms of regional uplift since the Mesozoic, related to the anomalous height of southern Africa, are contentious;
119 with landscape evolution either associated to mantle plumes (Nyblade and Robinson, 1994, Ebinger and Sleep, 1998) or to
120 plate tectonics, with uplift along flexures (Moore et al., 2009) and epeirogenic uplift (Brown et al., 1990). Furthermore, the
121 occurrence and timing of later Cenozoic uplift is disputed (e.g., Brown et al., 2002; van der Beek et al., 2002). Burke (1996)
122 proposed that the most recent uplift phase occurred ~30 Ma ago due to a thermal anomaly. Green et al. (2016) also argued for
123 Cenozoic uplift within southern South Africa that caused localised incision of the Gouritz River into the Swartberg mountain
124 range. However, Partridge and Maud (1987) argued for two phases of uplift during the Neogene, with a phase around 18 Ma
125 and a more recent phase at 2.58 Ma.

126

127 Figure 3 provides an overview of published geochronological studies in southern South Africa that used either apatite (U-
128 Th)/He and apatite fission track analysis to document landscape denudation from the Cretaceous to modern day, or in-situ
129 produced cosmogenic radionuclides (^{26}Al , ^{10}Be , ^3He , ^{21}Ne) to date landforms. Apatite (U-Th)/He and fission track data (Fig.
130 3) indicate high rates of denudation (up to 175 m My^{-1} , Tinker et al., 2008b) with respect to the present day rates, towards the



131 end of the Lower Cretaceous (100– 80 Ma) that decreased to up to 95 m My^{-1} by the late Cretaceous (90– 70 Ma; Brown et
132 al., 2002). Flowers and Schoene (2010) report negligible erosion since the Cretaceous, with rates as low as 5 m My^{-1} by the
133 late Eocene (36 My; Cockburn et al., 2000). Cosmogenic studies support low erosion rates within southern South Africa since
134 the start of the Cenozoic (Fig 3; Fleming et al., 1999; Cockburn et al., 2000; Bierman and Caffee, 2001; van der Wateren and
135 Dunai, 2001; Kounov et al., 2007; Codilean et al., 2008; Dirks et al., 2012; Decker et al., 2011; Erlanger et al., 2012; Chadwick
136 et al., 2013; Decker et al., 2013; Scharf et al., 2013; Bierman et al., 2014; Kounov et al., 2015). The majority of landforms are
137 eroding very slowly, with mean denudation rates ranging between 9.4 m My^{-1} for the escarpment faces to 0.85 m My^{-1} for
138 pediments (Fig. 3), although one reported retreat rate of 62.3 m My^{-1} have been measured for escarpment face retreat (Fleming
139 et al., 1999). In contrast, the Great Escarpment in the South African interior has higher fluvial incision rates than southern
140 South Africa: cosmogenic ^3He channel bed denudation rates range between 14 and 255 m My^{-1} and valley side and valley top
141 denudation rates range between 11 to 50 m My^{-1} for the Klip and Mooi Rivers and Schoonspruit, tributaries of the Orange
142 River (Keen-Zebert et al., 2016).
143



144

145 **Figure 3: Published exhumation and denudation rates for southern Africa. A) Apatite fission track and (U-Th)/He data**
 146 **show large variation in exhumation rates since the Cretaceous, and include data from Gallagher and Brown, 1999;**
 147 **Cockburn et al. 2000; Brown et al. 2002; Tinker et al. 2008b; Kounov et al. 2009 and; Flowers and Schoene, 2010. B)**
 148 **In-situ produced cosmogenic (¹⁰Be, ²⁶Al, ²¹Ne and ³He) nuclide-derived denudation rates for escarpment, pediment**
 149 **and fluvial landforms. Cosmogenic data is from the following sources; Flemming et al. 1999; Cockburn et al. 2000;**
 150 **Bierman and Caffee, 2001; van der Wateren and Dunai, 2001; Kounov et al. 2007; Codilean et al. 2008; Dirks et al.**
 151 **2012; Decker et al. 2011; Erlanger et al. 2012; Chadwick et al. 2013; Decker et al. 2013; Scharf et al. 2013; Bierman et**
 152 **al. 2014; and Kounov et al. 2015.**
 153

154 Southern South Africa, below the Great Escarpment, is currently tectonically quiescent with only minor Quaternary-active
 155 faults (Bierman et al., 2014) and low denudation and sediment production rates (Kounov et al., 2007; Scharf et al. 2013).
 156 Minimum exposure ages for pediments range from 0.29 +/- 0.02 Ma (Bierman et al., 2014) to 5.18 +/- 0.18 Ma (Van der
 157 Wateren and Dunai, 2001) with a mean minimum exposure age of 1.87 Ma (Pleistocene, van der Wateren and Dunai, 2001;
 158 Bierman et al., 2014; Kounov et al., 2015).

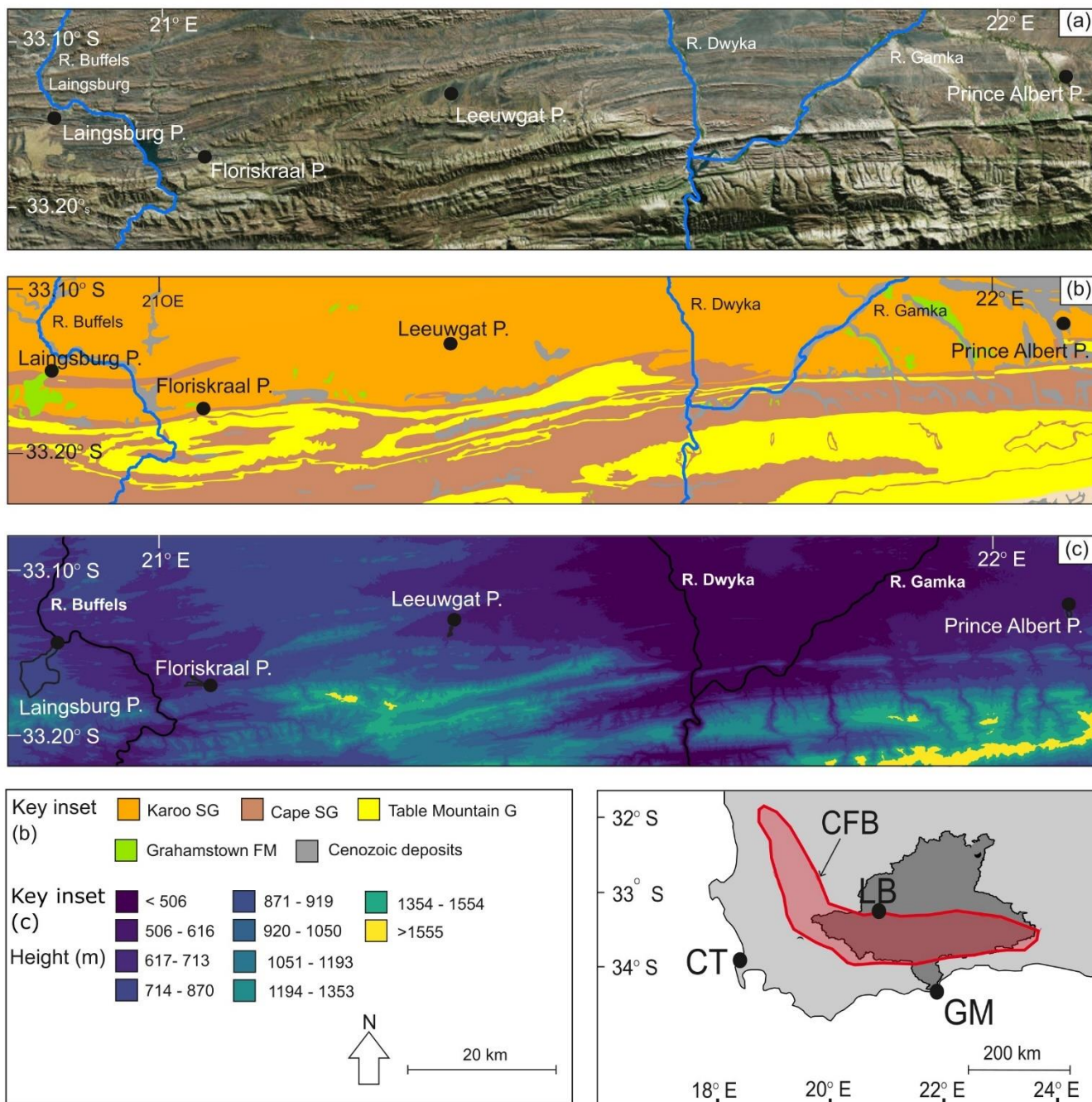


159

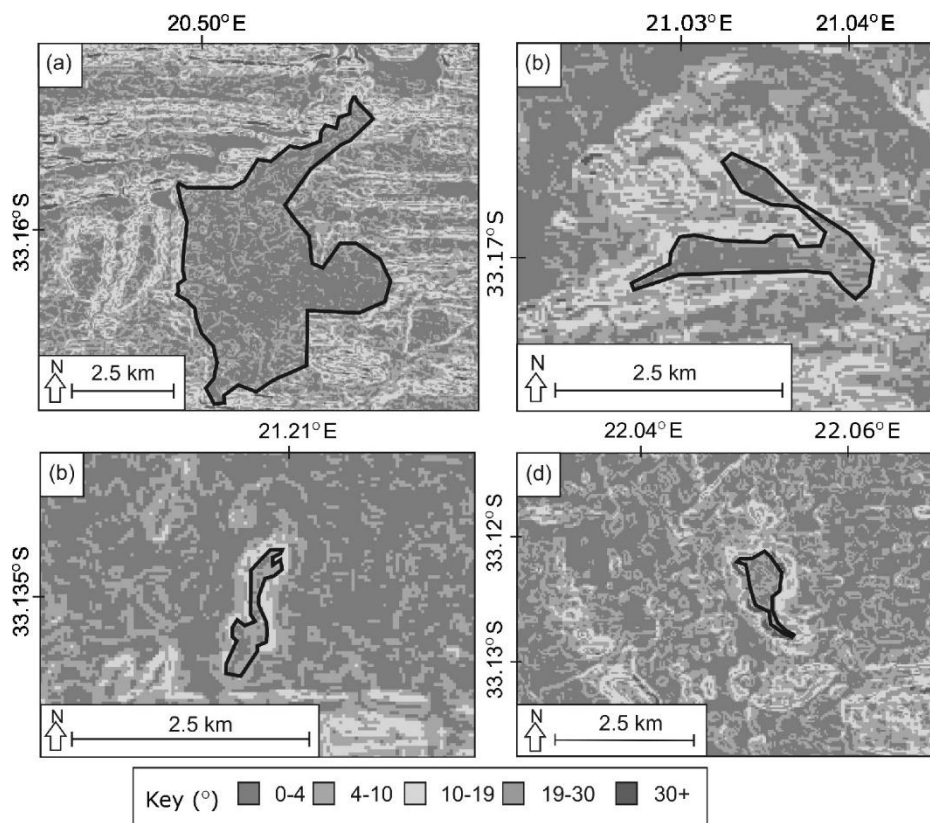
160 The climate of southern South Africa has gradually moved towards more arid conditions since the Cretaceous (Partridge, 1997;
161 van Niekerk et al., 1999) with an abrupt change from humid/tropical to arid conditions at the end of the Cretaceous (Partridge
162 and Maud, 2000) as shown by silcrete formation and saline soils (Partridge and Maud, 1987). Although there is general
163 agreement about the overall aridification trend since the Cretaceous, several authors have argued that wetter phases occurred
164 from 65 – 30 Ma (Burke, 1996), or that the arid phase started as late as 18 Ma (Partridge and Maud, 1987). The present day
165 climate of the Western Cape is primarily semi-arid (Dean et al., 1995), while the coastal region has a Mediterranean type
166 climate (Midgley et al., 2003).

167 **2.2 Sample Sites**

168 The sampling sites are located within the large antecedent Gouritz catchment (Fig. 4), where morphometric analysis has
169 identified the presence of flat surfaces or pediments that carry a thin sedimentary cover, hereafter called alluviated pediments
170 (<1m) (Richardson et al., 2016). The alluviated pediments grade away from the Cape Fold Belt (CFB) into adjacent alluvial
171 plains, and samples were collected from pediments on the northern flank of the Swartberg and Witteberg Mountains (CFB)
172 around Laingsburg, Floriskraal, Leeuwgat, and Prince Albert (Fig. 4a). Samples were taken from five deeply dissected
173 alluviated pediments ranging in surface area between < 1 to 20 km² and displaying slope angles below 10°, with most of the
174 slopes below 4° (Fig. 5).



175
 176 **Figure 4: (a) Pediment locations, the inset shows the location of the Gouritz catchment within South Africa, where CT**
 177 **– Cape Town, LB – Laingsburg; GM – Gouritzmond and the red polygon is the location of the Cape Fold Belt (CFB);**
 178 **(b) underlying geology below the pediments and; (c) pediment elevations (in m a.s.l.) as shown by elevation bins**
 179 **categorised by natural breaks in the elevation data.**
 180



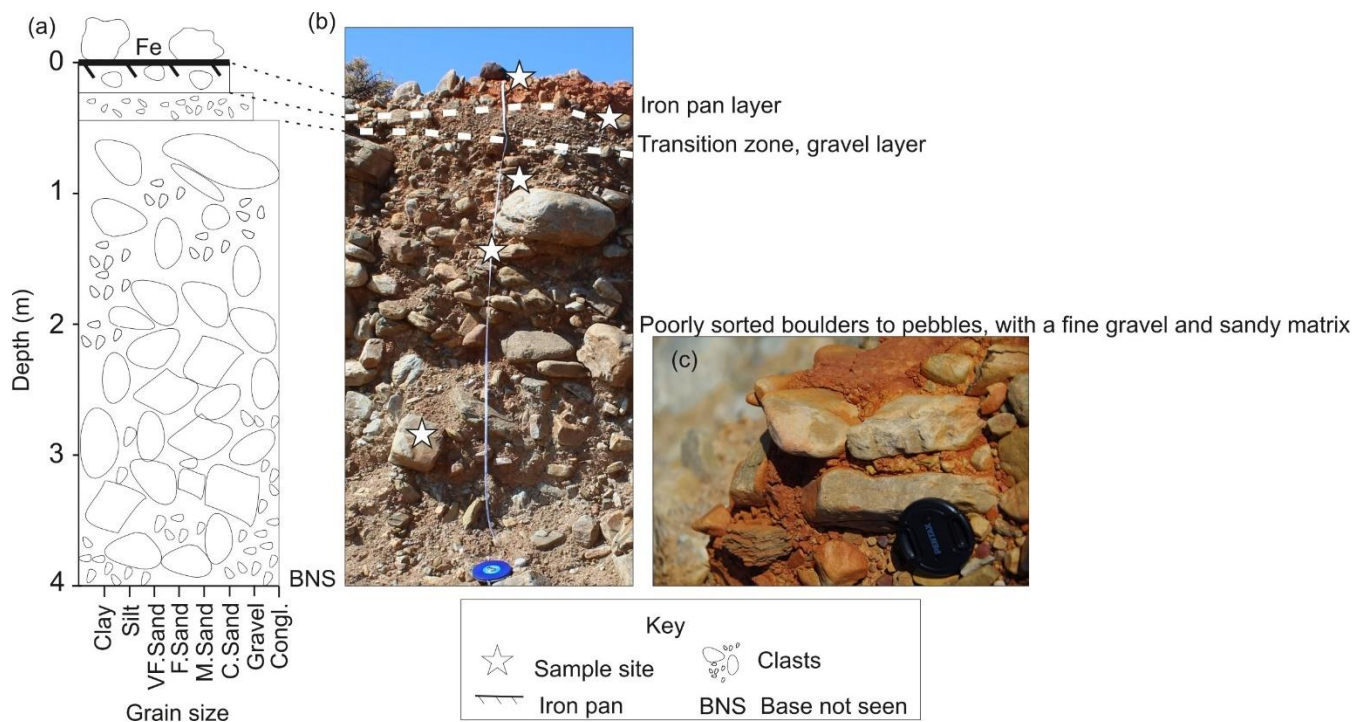
181

182 **Figure 5: Pediment slope data (with slope given in °); (a) Laingsburg; (b) Floriskraal; (c) Leeuwgat and; (e) Prince**
183 **Albert. For pediment locations please see Figure 4.**

184

185 The alluviated pediments are composed of unconsolidated, poorly-sorted gravel to boulder material in a matrix of sand (Fig.
186 6) that unconformably overlie folded rocks of the Karoo Supergroup (Fig. 3b). Some pediments are capped by silcrete, calcrete
187 or ferricrete (Helgren and Butzer, 1977; Summerfield, 1983; Marker and Holmes, 1999; Partridge, 1999; Partridge and Maud,
188 2000; Marker et al., 2002). Ferricrete is dominant on the Laingsburg pediment. The silcrete is assigned to the Grahamstown
189 Formation (Fig. 4b) that has poor age control (Mountain, 1980; Summerfield, 1983) due to the lack of formal identification of
190 the extent of the silcretes. Electron spin resonance ages for two silcrete caps in the Kleine Karoo were dated at 7.3 and 9.4 Ma
191 (Hagedorn, 1988).

192



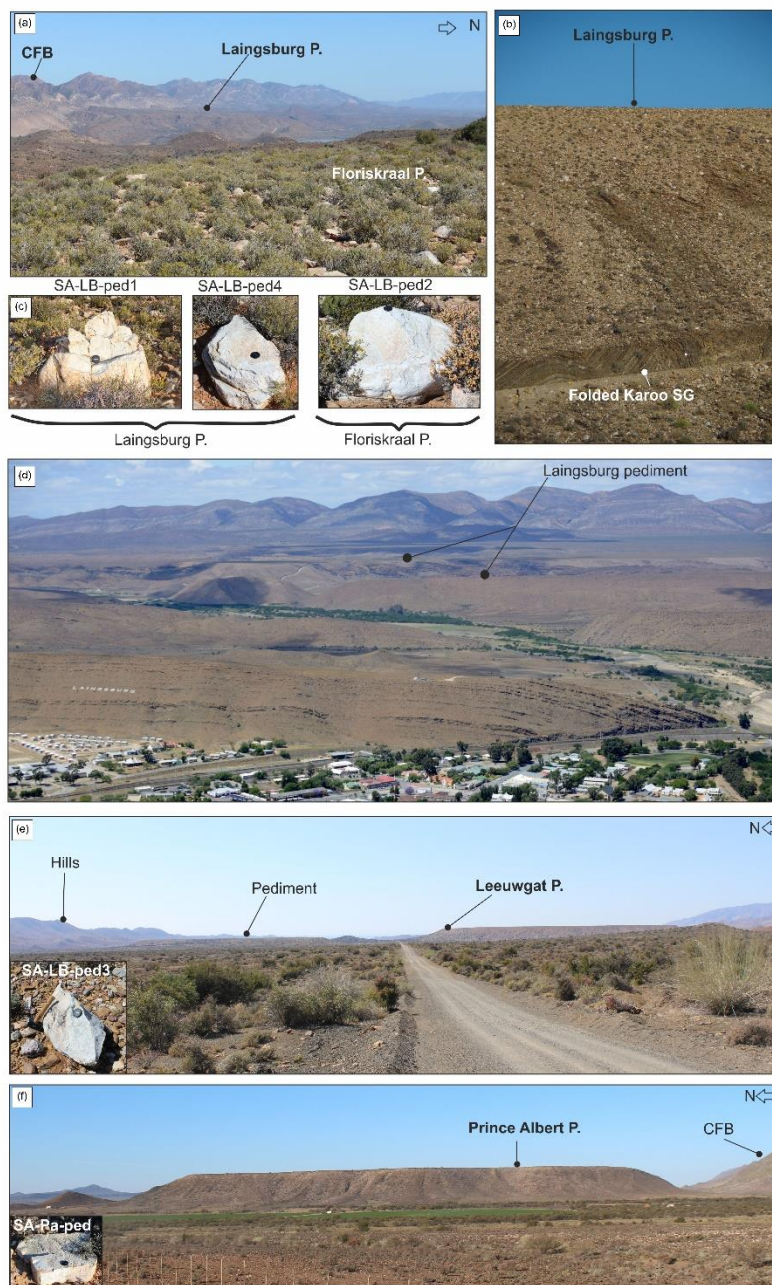
193

194 **Figure 6: (a) Sedimentary log of the Laingsburg pediment showing the unsorted boulders (dominantly quartzite) to**
195 **gravel size material; (b) photograph of the pediment and where the depth profile clasts were taken; (c) iron-rich**
196 **palaeosol layer.**

197 3. Methodology

198 3.1 Cosmogenic radionuclide dating

199 Two types of samples were collected for CRN analyses in 2014: five rock samples from alluviated pediment surfaces and
200 clasts from one depth profile in the Laingsburg pediment (Fig. 7, Table 1). Quartzite boulders from the Table Mountain
201 Group (Cape Supergroup) that were sampled at the surface of the pediments have a >1m diameter along their longest axis.
202 For the depth profile in the pediment, quartzite clasts (>25 cm diameter) were taken at the following depths (cm) below
203 ground level: 0, 30, 85, 150, 255 (Table 1).



204

205 **Figure 7: Sample sites; (a) Laingsburg pediment from the Floriskraal pediment; (b) Laingsburg pediment and**
206 **contact with underlying folded Karoo Supergroup (SG) strata; (c) Boulder samples from Laingsburg and Floriskraal**
207 **pediments; (d) large-scale picture of the Laingsburg pediment; (e) Leeuwgat pediment and boulder sample (inset); (f)**
208 **Prince Albert and boulder sample (inset). The figure also shows the dissection of the pediments by small river**
209 **catchments and how decoupled the Floriskraal and Prince Albert pediments are from the Cape Fold Belt.**



210 **Table 1: Site-specific information of the sampling sites for cosmogenic radionuclide analysis. All samples are taken**
 211 **from quartzite boulders, that were sampled either on the surface of the pediment (sample type = surf) or at depth**
 212 **(sample type = depth). The density of the sample or overburden (for depth samples) has been determined based on**
 213 **published density data of quartzite boulders and depth profiles in pediments by respectively Scharf et al. (2013) and**
 214 **Kounov et al. (2015).**

Sample ID	Sample type	Name	Latitude (°S)	Longitude (°E)	Elevation (m)	Density (g/cm ³)	Topographic Shielding	Cover correction
SA-PA_ped	Surf	Prince Albert	33.203	22.082	703	2.7	1.00	NA
SA-LB_ped1	Surf	Laingsburg	33.246	20.872	764	2.7	1.00	NA
SA-LB_ped2	Surf	Floriskraal	33.285	21.050	706	2.7	1.00	NA
SA-LB_ped3	Surf	Leeuwgat	33.221	21.347	691	2.7	1.00	NA
SA-LB_ped4	Surf	Laingsburg	33.261	20.854	791	2.7	1.00	NA
SA-LB_DP0	Depth	Laingsburg	33.256	20.851	779	1.6	0.99	NA
SA-LB_DP30	Depth	Laingsburg	33.256	20.851	776	1.6	0.99	0.79
SA-LB_DP85	Depth	Laingsburg	33.256	20.851	776	1.6	0.99	0.54
SA-LB_DP150	Depth	Laingsburg	33.256	20.851	776	1.6	0.99	0.37
SA-LB_DP255	Depth	Laingsburg	33.256	20.851	776	1.6	0.99	0.23

215

216 The samples were processed for in-situ cosmogenic ¹⁰Be following standard methods as described in von Blanckenburg (2004)
 217 and Vanacker et al. (2007). Rock samples were crushed, sieved and rock fragments of 250 to 500 µm diameter were selected
 218 for further lab processing. Quartz minerals were extracted by chemical leaching with a low concentration of acids (HCl, HNO₃,
 219 and HF) in an overhead shaker. Purified quartz samples were then leached with 24% HF for 1h to remove meteoric ¹⁰Be,
 220 followed by spiking the sample with 150 µg of ⁹Be and total decomposition in concentrated HF. The Beryllium in solution
 221 was extracted by ion exchange chromatography as described in von Blanckenburg et al. (1996). The ¹⁰Be/⁹Be ratios were
 222 measured using accelerator mass spectrometer on the 500 kV Tandy facility at ETH Zürich (Christl et al., 2013). Measured
 223 ¹⁰Be/⁹Be ratios were normalised to the ETH in-house secondary standard S2007N with a nominal ratio of 28.1×10⁻¹² (Kubik
 224 and Christl, 2010), which is in agreement with a ¹⁰Be half-life of 1.387 Ma (Chmeleff et al., 2010). Sample ratios were blank
 225 corrected ($7.54 \pm 9.67 \times 10^{-15}$) and the analytical uncertainties on the ¹⁰Be/⁹Be ratios of blanks and samples were then
 226 propagated into the 1σ analytical uncertainty for the ¹⁰Be concentrations (Table 2 and 3). Production rates were scaled
 227 following Dunai (2000) with a sea level high-latitude production rate of 4.28 atoms g_{qtz}⁻¹ yr⁻¹. The bulk density was set to 2.7
 228 g cm⁻³ for samples from quartzite boulders following Scharf et al. (2013), and to 1.6 g cm⁻³ for the overburden of the depth
 229 samples following earlier work on depth profiles in the Western Cape by Kounov et al. (2015). The concentrations were
 230 corrected for topographic shielding using the procedure described in Norton and Vanacker (2009).



231 **Table 2 : Cosmogenic nuclide data for depth profile in Laingsburg. The reported ^{10}Be concentrations are corrected for**
 232 **procedural blanks, using a value of $7.54 \pm 9.67 \times 10^{-15}$, and the 1σ uncertainty estimates contain analytical errors from**
 233 **AMS measurement and blank error propagation.**
 234

Sample ID	Depth (cm)	^{10}Be concentration ($\pm 1\sigma$), ($\times 10^6$ at/g _{qtz})
SA-LB_DP0	0	5.460 ± 0.106
SA-LB_DP30	30	1.196 ± 0.111
SA-LB_DP85	85	0.893 ± 0.036
SA-LB_DP150	150	0.376 ± 0.016
SA-LB_DP255	255	0.133 ± 0.015

235

236

237 **Table 3: Cosmogenic nuclide data for surface samples from pediments. The reported ^{10}Be concentrations are corrected**
 238 **for procedural blanks, using a value of $7.54 \pm 9.67 \times 10^{-15}$, and the 1σ uncertainty estimates contain analytical errors**
 239 **from AMS measurement and blank error propagation. Maximum denudation rates and minimum durations of surface**
 240 **exposure were calculated using the CosmoCalc add-in for Excel (Vermeesch, 2007). For the surface exposure ages, we**
 241 **assumed (1) no erosion or burial since exposure, and (2) a maximum steady erosion rate of 0.3 m My^{-1} .**
 242

Sample ID	Location	^{10}Be concentration ($\times 10^6$ at/g _{qtz}) ($\pm 1\sigma$)	^{10}Be denudation rate (m My^{-1}) ($\pm 1\sigma$)	Minimal exposure age (My) ($\pm 1\sigma$)	
				No erosion or deposition	Erosion rate of 0.30 m My^{-1}
SA-PA_ped	Prince Albert	2.834 ± 0.055	0.954 ± 0.025	0.569 ± 0.010	0.678 ± 0.010
SA-LB_ped1	Laingsburg	5.199 ± 0.096	0.408 ± 0.013	1.131 ± 0.016	1.964 ± 0.016
SA-LB_ped2	Floriskraal	5.148 ± 0.095	0.383 ± 0.013	1.189 ± 0.016	2.220 ± 0.016
SA-LB_ped3	Leeuwgat	5.641 ± 0.103	0.315 ± 0.011	1.377 ± 0.018	4.462 ± 0.018
SA-LB_ped4	Laingsburg	4.252 ± 0.067	0.587 ± 0.014	0.848 ± 0.011	1.164 ± 0.010
SA-LB_DP0	Laingsburg	5.460 ± 0.106	0.373 ± 0.013	1.210 ± 0.018	2.333 ± 0.018

243

244



245 For the derivation of the minimum durations of exposure (Table 3), we used two different scenarios: a hypothetical case
246 assuming no erosion or burial since exposure, and a second case assuming steady erosion of the pediment surface of 0.3m My⁻¹
247 following Bierman et al. (2014). The CosmoCalc method, version 3.0 (Vermeesch, 2007) was employed to calculate
248 maximum denudation rates and minimum surface exposure ages from the ¹⁰Be concentrations of the surface samples (Table
249 3). The surface exposure ages are *minimum estimates* as isotopic steady state can be reached for old material.

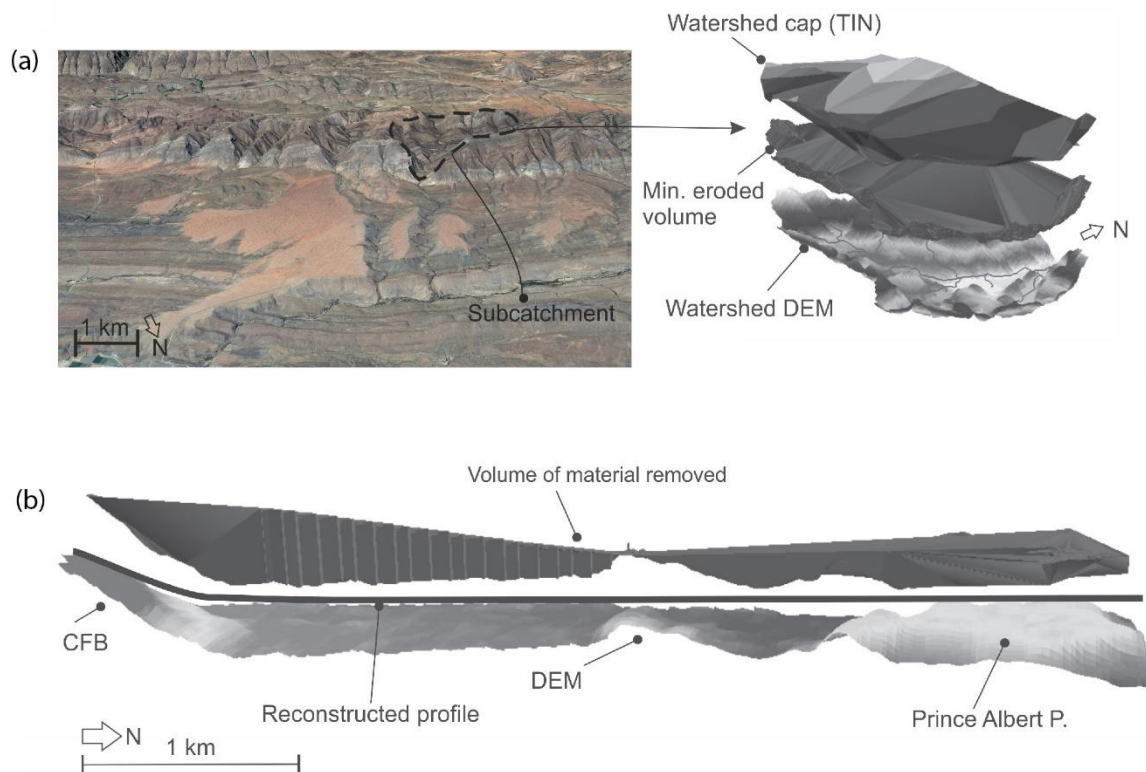
250 In addition, we use a concentration depth profiling approach to better constrain the exposure and denudation of the Laingsburg
251 area pediment. The accumulation of ¹⁰Be, $N_{\text{total}}(z,t)$, in the eroding surface of the pediments can be described as:

$$252 \quad N(z, t) = N_{\text{inh}} e^{-\lambda t} + \sum_i \frac{P_i(z)}{\lambda + \frac{\rho E}{\Lambda_i}} e^{-\rho(z_0 - Et)/\Lambda_i} \left(1 - e^{-\left(\lambda + \frac{\rho E}{\Lambda_i}\right)t} \right) \quad \text{Eq.1}$$

253 where E is expressed in cm/yr ($\text{m/Myr} \times 10^4$), t [yr] is the exposure age, λ [1/yr] the nuclide decay constant ($\lambda = \ln 2 / t_{1/2}$), z_0
254 (cm) the initial shielding depth ($z_0 = E \times t$), ρ [g/cm^3] the density of the overlying material, and Λ_i [g/cm^2] the attenuation
255 length. The production rate, $P_i(z)$ [atoms/g/yr], is a function of the depth, z [cm], below the surface. The subscript ‘i’ indicates
256 the different production pathways of ¹⁰Be via spallation, muon capture and fast muons following Dunai (2010). In this study,
257 the relative spallogenic and muogenic production rates are based on the empirical muogenic-to-spallogenic production ratios
258 established by Braucher et al. (2011), using a fast muon relative production rate at SLHL of 0.87% and slow muon relative
259 production rate at SLHL of 0.27%. The attenuation length was set to 160, 1500 and 4320 g cm^{-2} for the production by,
260 respectively, neutrons, negative muons and fast muons (Braucher et al., 2011). The depth profile is then solved numerically,
261 based on a chi-squared model fitting between the observed (Table 2) and simulated ¹⁰Be concentrations at different depths.

262 3.2 Morphometric Analysis

263 Aster 30m data was used to build a DEM of the study area in ArcGIS 10.1. The DEM was re-projected into WGS 1984 world
264 Mercator co-ordinates and filled using the hydrology toolbox. The drainage was extracted using an upstream contributing
265 area of 3.35 km^2 , and both ephemeral and perennial streams were delineated (e.g., Abadelkaarem et al., 2012; Ghosh et al.,
266 2014). Dissected pediments were derived using a method adapted from Bellin et al. (2014). The previous grading from the
267 mountain front was reconstructed for each pediment in ArcGIS (Fig. 8). This surface was then placed into ArcScene 10.1, with
268 the difference between the reconstructed surface and the current topography (using the DEM) providing a minimum volume
269 of material removed after pediment formation. A similar approach was applied to derive bulk erosion volumes for the small
270 sub-catchments that back the pediment surfaces in the CFB. The bulk erosion is likely to be a minimum estimate of the total
271 rock volume removed by erosion, as interfluvial erosion might have occurred (Bellin et al., 2014; Brocklehurst and Whipple,
272 2002). Eroded volumes were then converted to lithological thickness using the method of Aguilar et al. (2011).



273

274 **Figure 8: Examples of (a) bulk eroded volumes from subcatchments and (b) cross section of the Prince Albert**
275 **pediment showing the method used in ArcGIS for the volume of material removed around the pediment surface.**

276 4. Results

277 4.1 Alluviated pediment composition

278 The contact with the underlying bedrock (e.g., Dwyka Group) is erosional and undulating, it is not a smooth planation contact.
279 The alluviated pediments are composed of poorly sorted boulders to pebbles, with a matrix of sandy gravel. The clasts are
280 predominantly quartzites (Table Mountain Group); however smaller clasts of Dwyka Group lithologies are present. Towards
281 the top of the profile there is a small transition zone of gravel, which is capped by an iron crust (Fig. 6). There is no indication
282 of fluvial activity (i.e., imbrication). There is no grading or sediment clast size variation throughout the profile, and the clasts
283 range from sub-rounded to sub-angular.

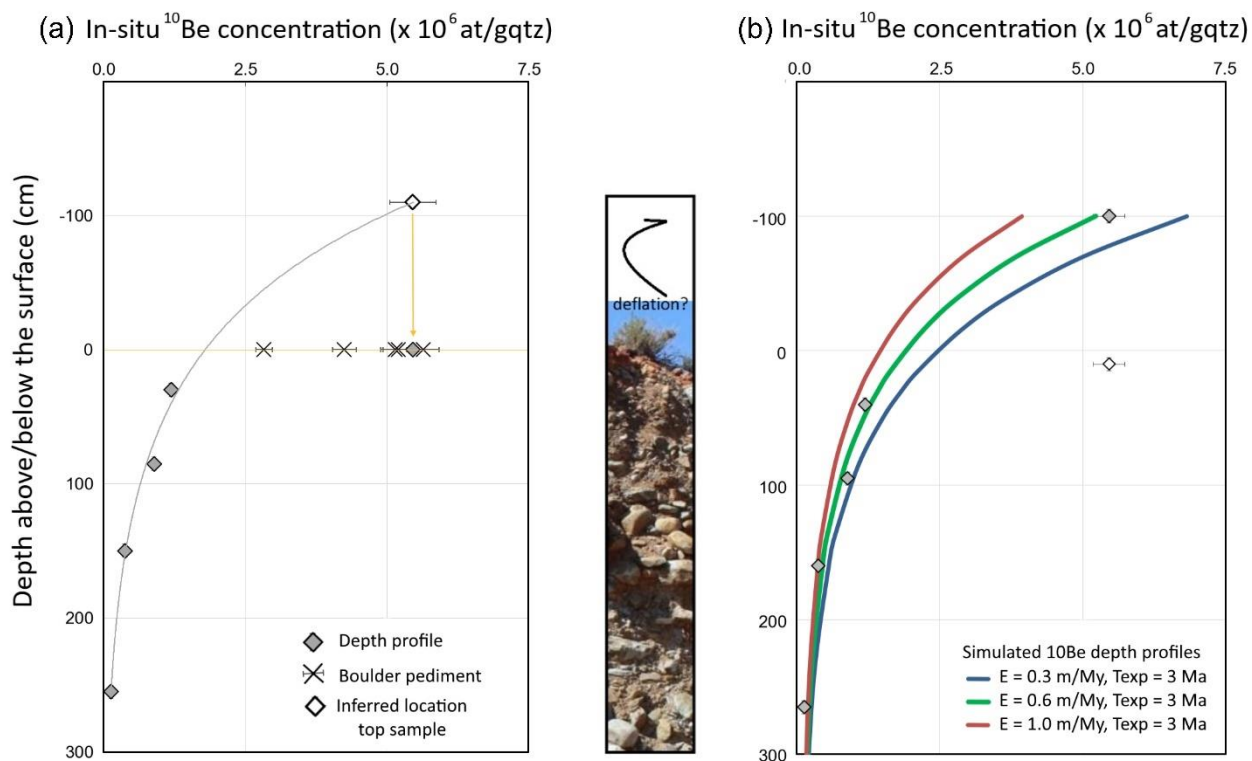
284



285 4.2 Cosmogenic nuclides

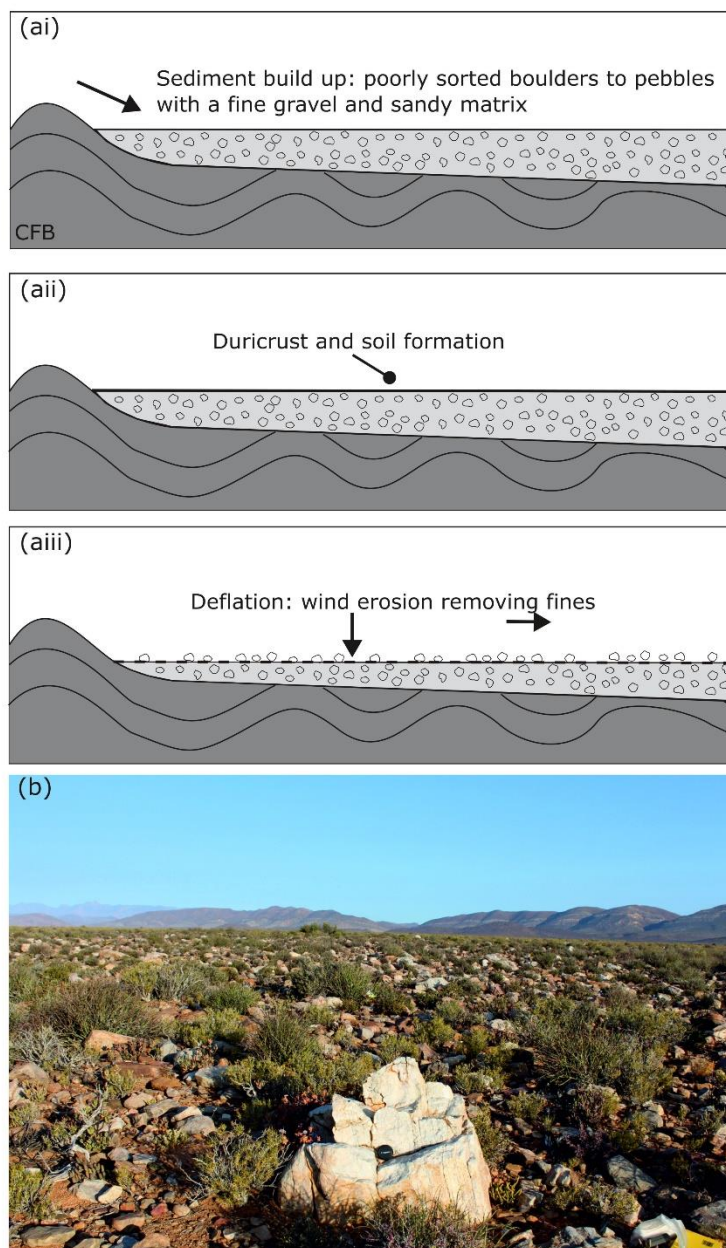
286 The surface lowering rates (Table 3) calculated for the boulders sampled on the pediment surface show very low maximum
287 denudation rates, which range from 0.315 to 0.954 m My⁻¹. The Laingsburg area alluviated pediment has higher rates of surface
288 lowering closer to the CFB, with denudation rates decreasing towards the proximal part of the pediment as shown by the
289 boulder samples. The alluviated pediment in the Prince Albert area has the highest rate of maximum surface lowering (0.954
290 m My⁻¹), which is an order of magnitude higher than the average surface lowering rate of the other studied alluviated pediments.
291 The minimum exposure ages assuming no erosion or burial (Table 3) indicate that the alluviated pediments are long-lived,
292 with *minimum* surface exposure ages between 0.569 and 1.377 My (Pleistocene). The Prince Albert area alluviated pediment
293 has the youngest *minimum* exposure age of 0.569 My, the Laingsburg area pediment has variable minimum exposure ages
294 from 0.848 to 1.131 My. Over this timeframe, the assumption of no erosion or deposition is an unlikely scenario. Assuming
295 low erosion rates of 0.3 m My⁻¹ the pediment minimum exposure ages increase substantially for the older surfaces, with
296 minimum ages ranging from 0.678 to 4.462 My (Table 3).

297 The ¹⁰Be concentration depth profile provides more insights in the denudation process of the pediments. First, the uppermost
298 sample of the Laingsburg depth profile has a ¹⁰Be concentration that is in line with the concentrations that are measured in
299 boulders sampled at the Laingsburg, Floriskraal and Leeuwgat alluviated pediments, and is markedly higher than the
300 concentration measured at the Prince Albert alluviated pediment (Fig. 9a, Table 3). Second, there is a large discrepancy in the
301 ¹⁰Be concentrations between the uppermost sample and the four samples taken at depth in the profile (Table 2). The 4.265 ×
302 10⁶ at./g difference in ¹⁰Be concentrations over a 30 cm depth increment cannot be explained by steady erosion of the pediment
303 after exposure (Fig. 9b). It suggests that deflation of ~110 cm of fine-grained material at the surface of the pediments has
304 resulted in a pavement of old boulders at the top of a slowly eroding surface (Fig. 10).



305

306 **Figure 9: Depth profile results of the Laingsburg pediment. (a) showing depth profile data and (b) showing erosion**
307 **rate scenarios.**



308

309 **Figure 10: (a) Process of deflation and (b) Evidence of deflation: concentrations of boulders and pebbles on top of the**
310 **Laingsburg Pediment.**

311

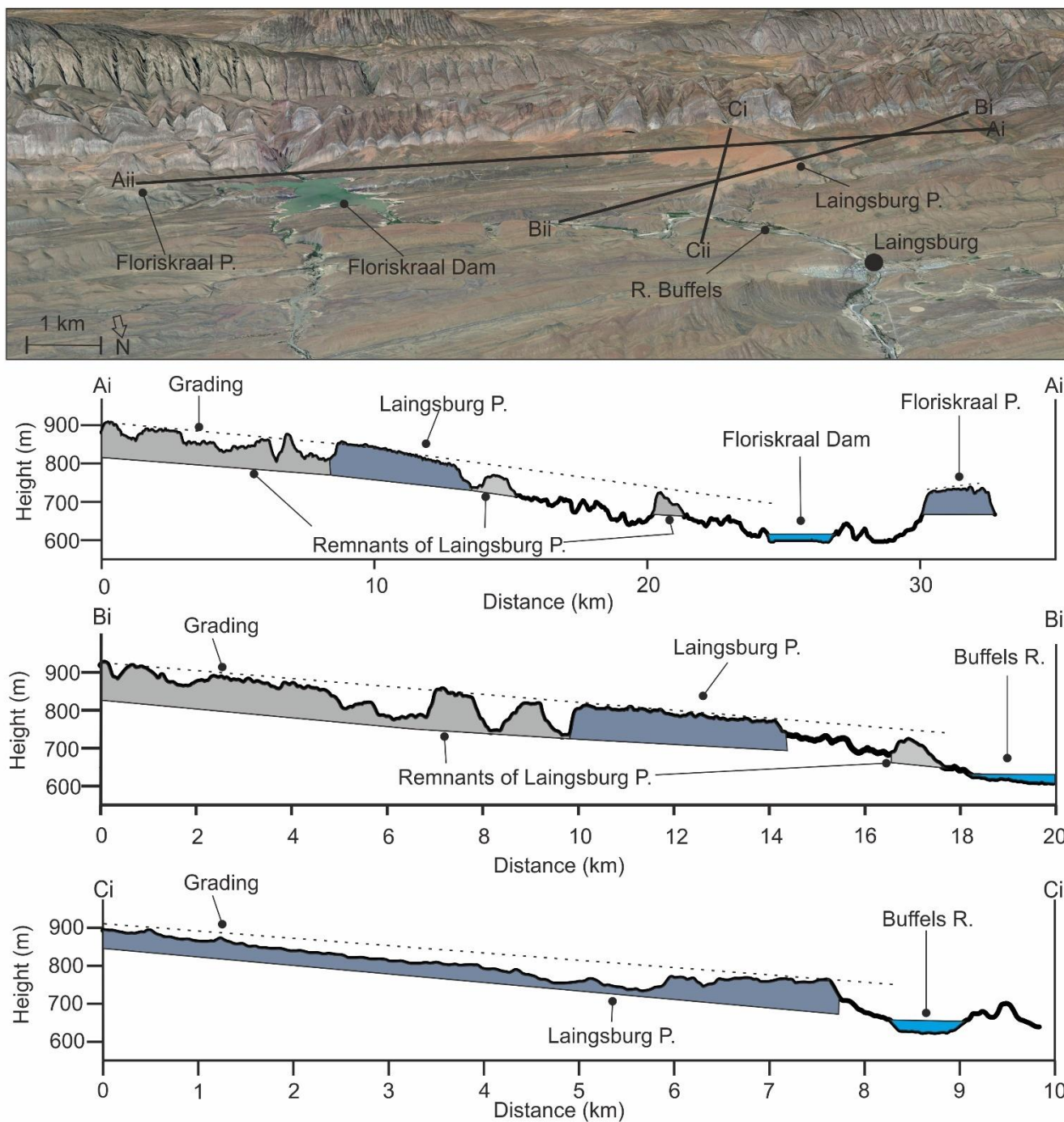


312 When taking ablation of the upper ~110cm of the profile into account, the ^{10}Be concentration depth profile of the Laingsburg
313 pediment can be simulated by forward modelling (Vandermaelen et al., 2022) using minimum age constraints from the surface
314 samples and information on the density of the overlying material from Kounov et al. (2015). The most likely denudation rate
315 of the pediment is ~0.6 m/My (Figure 9b), which is similar to the median erosion rate for South African pediment surfaces
316 reported by Bierman et al (2014). Even at this low surface lowering rate, the ^{10}Be concentrations approach isotopic steady state
317 when the time of exposure exceeds 3 Ma, so that the age information derived from the depth profile only provides a *minimum*
318 exposure age.

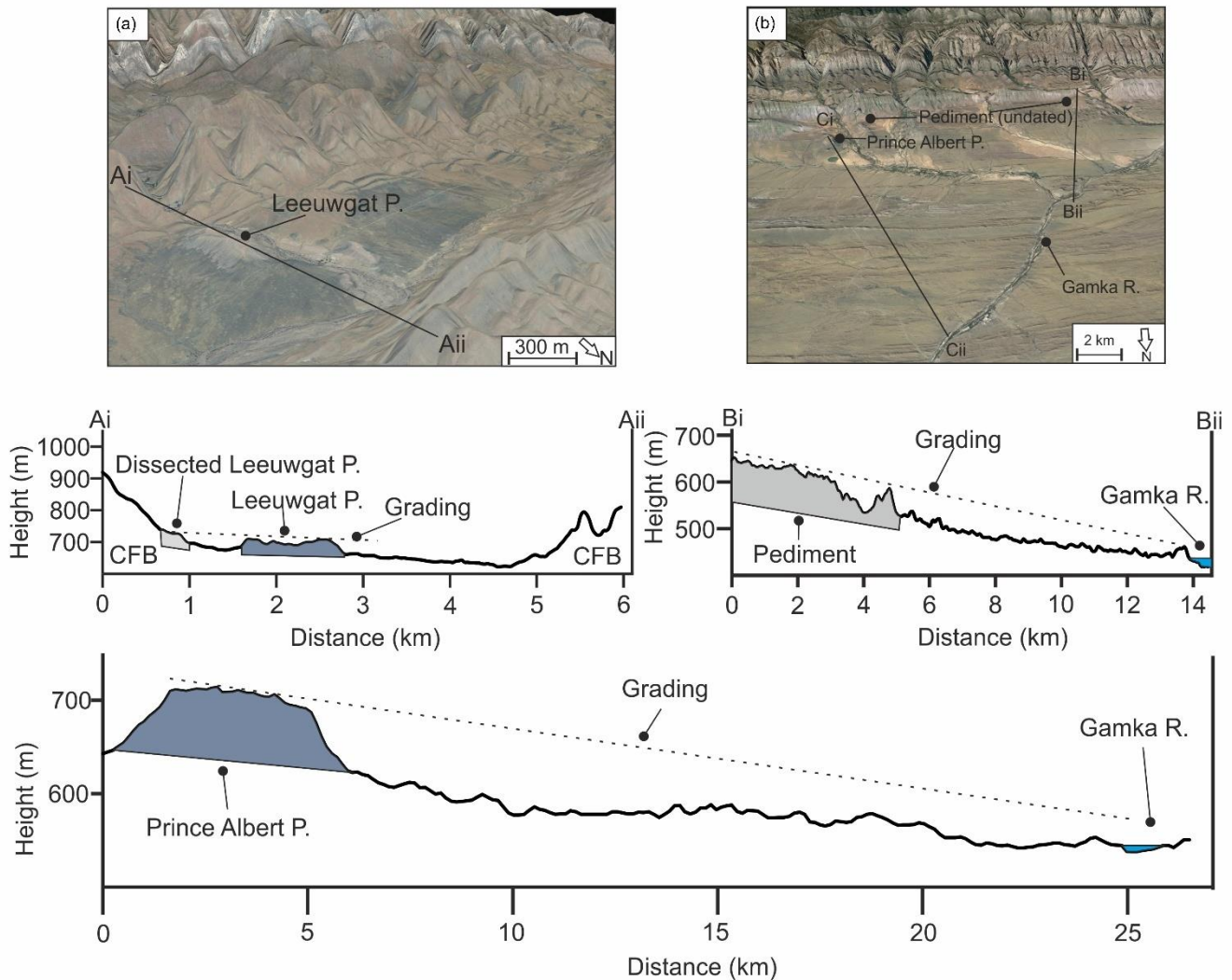
319 **4.3 Elevations and grading of pediment**

320 Figure 4c shows the pediment heights as classified by the Jenks natural break scheme (De Smith and Goodchild, 2007). The
321 alluviated pediments at Laingsburg and Floriskraal have elevations within the same class (714 – 870 m), and the Leeuwgat
322 and Prince Albert area alluviated pediments share the same elevation class (617 – 713 m). The Laingsburg area alluviated
323 pediment appears to have an aspect of slope that grades not only away from the CFB but towards the modern Buffels River
324 location, which abuts the northern limit of the alluviated pediment (Fig. 11). This relationship is less clear on the Floriskraal
325 alluviated pediment, which is to the east of the Buffels River. The alluviated pediment at Leeuwgat, which sits between two
326 folds of the CFB, has no large trunk river nearby (~30 km from Dwyka River) and simply grades away from the CFB (Fig.
327 12A). The Prince Albert area pediment grades towards the Gamka River, although it is currently ~16 km from the Gamka
328 River (Fig. 12b). The fact that the alluviated pediments grade towards the present day trunk rivers but above their present day
329 elevation indicates that these rivers were active during the formation of the pediments and is discussed later.

330



331
332 **Figure 11: Grading of the Laingsburg pediment and related cross sections, which grade not only away from the Cape**
333 **Fold Belt but towards the Buffels River.**
334



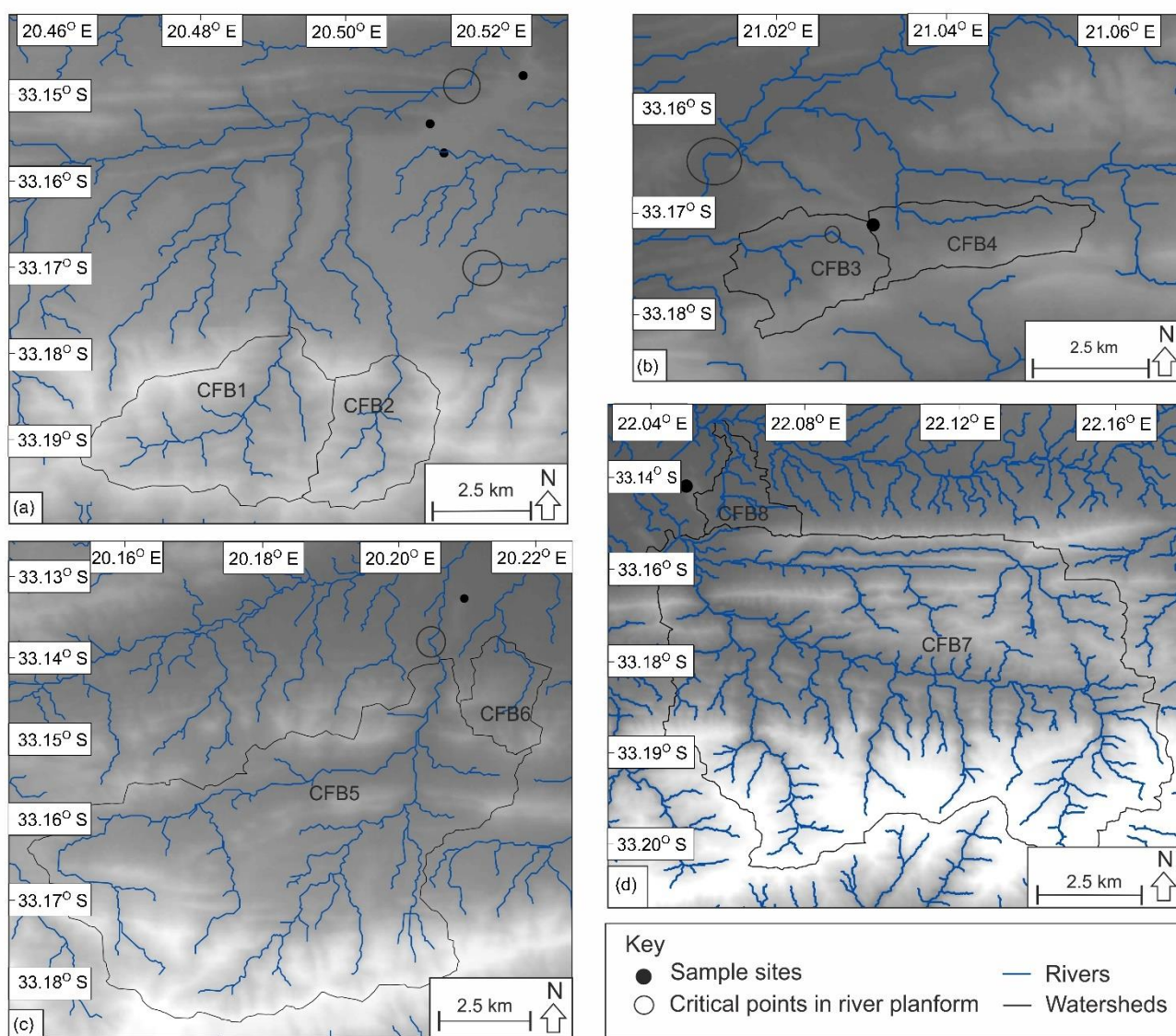
335
336 **Figure 12: Grading of the (a) Leeuwgat, which grades away from the Cape Fold Belt and (b) Prince Albert pediment,**
337 **which grades towards the Gamka River.**
338

339 4.4. Dissecting river planform

340 The dissecting river planforms are shown in Fig. 13. critical points are highlighted that relate to sections where the rivers (i)
341 have been deflected by the pediment surface, or (ii) have anomalous changes in orientation. Overall, the low order rivers (<4)
342 that have dissected the pediments are strongly influenced by the folding within the CFB (Richardson et al., 2016). This is
343 especially seen within the rivers that have dissected the Laingsburg pediment (Fig. 13a), where the linear river planform aligns



344 with the axis of a syncline. Where the rivers breach the folds it appears that the presence of alluviated pediments deflected the
345 river planforms; this relationship can also be seen at Floriskraal and Prince Albert area alluviated pediments (Fig. 13).



346

347 **Figure 13: Planforms of the dissecting rivers and Cape Fold Belt subcatchments; (a) Laingsburg; (b) Floriskraal; (c)**
348 **Leeuwgat and; (d) Prince Albert. The circles highlight critical points related to deflection of the river planforms by the**
349 **Cape Fold Belt or the pediment.**



350 **4.5 Volume of material removed**

351 Table 4 shows the bulk erosion rates related to dissection of the alluviated pediment post formation. Converting this to an
352 equivalent lithological thickness (dividing the volume of material removed over the area; Aguilar et al., 2011), an average of
353 141.43 m has been eroded around the large Laingsburg area pediment (Fig. 11). The Prince Albert area pediment, has an
354 average lithological thickness of 42.33 m removed. Leeuwgat has had the least amount of dissection, with 17.25 m eroded.

355 **Table 4: Minimum volume of material eroded by rivers incising the pediment surface, the equivalent rock thickness**
356 **and the time taken for incision using the average maximum denudation rate of 10.16 m My⁻¹ from Scharf et al., 2013**
357 **and Kounov et al., 2015.**

Location	Volume of material removed (km ³)	Equivalent average rock thickness (m)	Time for incision (Ma)
Laingsburg	3.240	141.43	13.92
Floriskraal	0.154	42.33	4.17
Leeuwgat	0.169	44.27	4.36
Prince Albert	0.012	17.25	1.70

358

359 Table 5 shows the volume of material eroded by rivers draining the sub-catchments in the CFB, which have dissected the
360 alluviated pediments. The sub-catchments range in area from 4.9 – 310 km², and the volume of material removed ranges from
361 0.11 - 89 km³, which is the equivalent of 21 - 286 m of lithological thickness. The alluviated pediments that are located further
362 away from the CFB range have larger dissecting catchments associated with them. For example, the Laingsburg area alluviated
363 pediment, which is backed by the CFB, has an average sub-catchment area of 14.37 km², whereas the Prince Albert area
364 alluviated pediment is located ~ 2 km from the CFB and has an average sub-catchment area of 161.83 km². These sub-
365 catchment areas are contributing to the incision of the pediments.

366

367

368

369

370

371



372 **Table 5: Minimum volume of material eroded by rivers draining the Cape Fold Belt sub-catchments, the equivalent**
373 **rock thickness and the average time taken for incision using the average of the maximum denudation rate recorded**
374 **from Scharf et al., 2013 and Kounov et al., 2015 of 10.16 m My⁻¹.**

Location	Catchment	Area (km ²)	Volume of material removed (km ³)	Equivalent average rock thickness (m)	Time for incision (Ma)
Laingsburg	CFB 1	19.79	2.86	144.39	14.21
	CFB 2	8.96	0.85	95.55	9.40
Floriskraal	CFB 3	6.21	0.28	45.31	4.46
	CFB 4	6.02	0.20	33.59	3.31
Leeuwgat	CFB 5	73.80	7.55	102.25	10.06
	CFB 6	4.91	0.11	21.64	2.13
Prince Albert	CFB 7	310.75	89.01	286.44	28.19
	CFB 8	12.92	0.23	17.79	1.75

375

376 5. Discussion

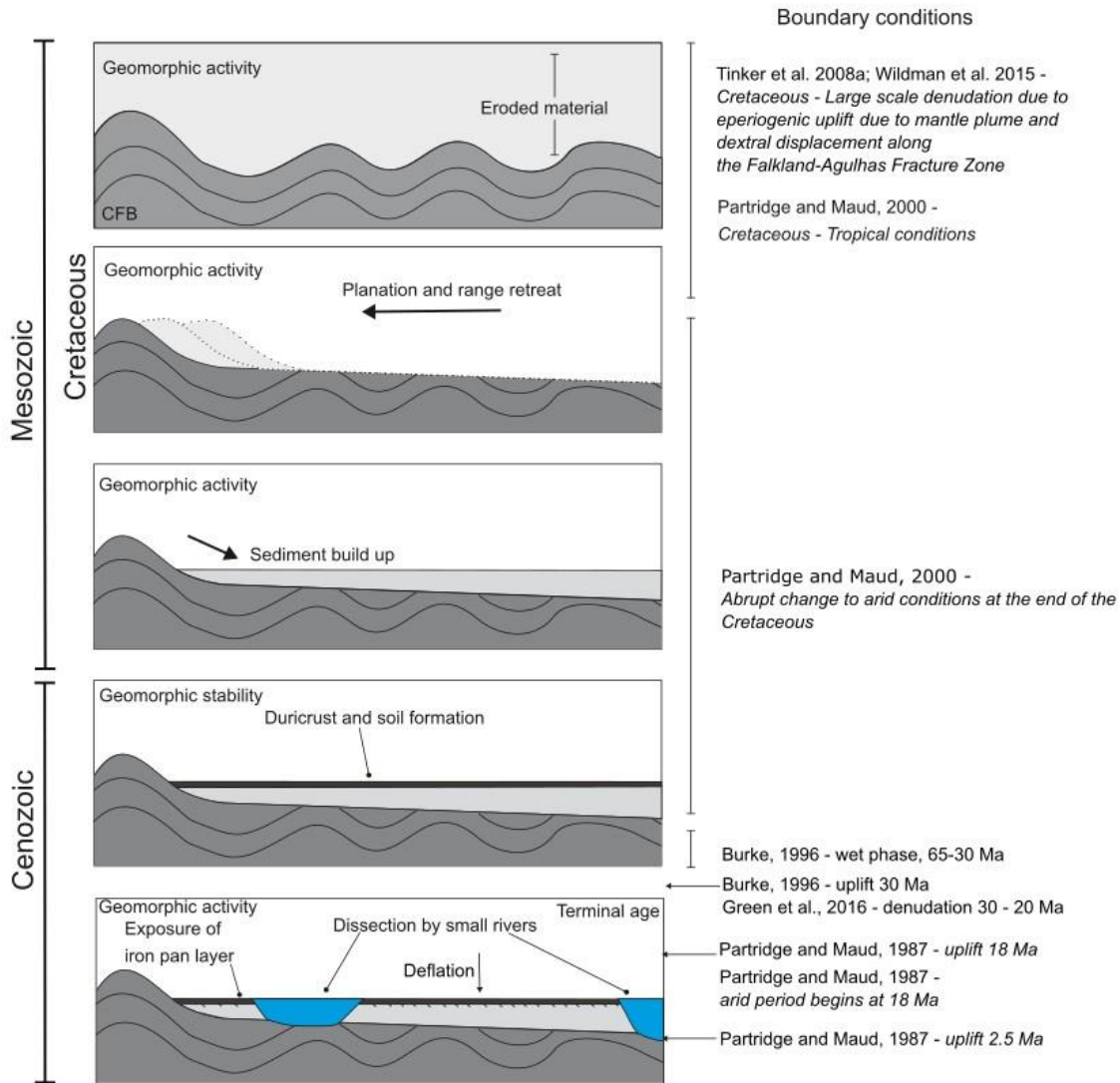
377 5.1 Pediment formation and characteristics

378 The pediments are underlain by folded strata of the Karoo and Cape Supergroups (sandstone, siltstone and mudstone), and
379 backed by the resistant CFB quartzites (Fig. 4b). It has been argued that pediments form on all lithology types, however the
380 more extensive pediments can be found above the least resistant material (Dohrenward and Parsons, 2009). There is no
381 systematic variation in pediment characteristics that can be related to the underlying geology (Fig. 4b).

382 The pediments have formed by diffusive processes, dominated by slope processes in the first stages of development, causing
383 the gradual retreat of the Cape Fold Belt and coeval formation of colluvial material and the weathering mantle, including an
384 iron pan (Fig. 14). There is no evidence of fluvial activity, such as clast imbrication, depositional or erosional bedforms, or
385 channel-forms (Fig. 6; *cf.* e.g., Gilbert, 1877; Sharp, 1940; Lustig, 1969). The iron pan layer is now at the surface of the
386 pediment due to the removal of overlying material as a result of surface deflation by wind erosion, as shown by the cosmogenic
387 data from the ¹⁰Be concentration depth profile (Figs. 9, 14). The pediments grade towards, but above, large trunk rivers of the
388 Gouritz catchment (Figs. 11, 12), indicating that large transverse systems were active before pediment planation and colluvial
389 build-up. The trunk rivers were also active during pediment formation, however they were probably less so, as shown by the
390 build-up and preservation of material forming the pediments. This suggests that at the time of pediment formation there was
391 deposition of colluvial material adjacent to large-scale sediment bypass via rivers, and formation of the pediment surfaces



392 because of erosion processes. The trunk rivers, active during the formation of the pediments represent an upper limit to the
 393 extent of the pediments and the pediments should be regarded as individual landforms and not as an extensive regional ‘surface’
 394 within the study area (*cf.* King, 1948, 1953, 1955; Partridge and Maud, 1987).



395

396 **Figure 14: Sequence of events forming the pediments and boundary conditions; in which the folded Karoo**
 397 **Supergroup strata was planned, hillslope processes caused the build-up of sediment, soil formation and duricrust**
 398 **formation. The pediments were then dissected and fluvial processes dominate. In recent time, deflation processes**
 399 **have dominated (Fig. 10).**



400 The distribution of the dissected pediments suggests that these are remnants of much more continuous local features (Fig. 12).
401 There has been a shift in the dominant process regime, from slope processes to fluvial processes, during the evolution of the
402 pediments as evidenced by the dissection of pediments by smaller rivers and the decoupling of the pediments from the CFB
403 sediment source area. The river planform has been primarily controlled by the orientation of tectonic folds. However, the
404 pediments could have also controlled the landscape evolution by deflecting the rivers, allowing the surfaces to be preserved.
405 It appears that the structural integrity of the pediment is not continuous across the entire pediment, and areas underlain by
406 cohesive material caused deflection of the dissecting rivers due to a higher resistance to erosion (Fig. 13). This could be a
407 function of the sedimentology (Fig. 6) of the pediment: the calibre of material; the extent of packing; or the presence and
408 thicknesses of the duricrust layer. Deflection of rivers has been shown to cause the formation of epigenetic gorges (Quimet et
409 al., 2008). Furthermore, the pediments could have been preserved in these locations as rivers did not migrate laterally, which
410 could be due to variations in channel gradient. The pediments sit above the valley floor (current level of erosion) and are
411 fossilised landforms that represent a store of sediment that is mostly subject to weathering and deflation under current climatic
412 conditions (Fig. 10), with hillslope processes slowly supplying sediment to the nearby fluvial channels; however due to slow
413 runoff rates related to the arid climate, the transport is no longer effective.

414

415 **5.2 Implications of depth profile**

416 The CRN concentration depth profile (Table 2) indicates that the ^{10}Be concentrations in the sedimentary sequence deviate from
417 a simple exponential concentration depth profile. The stronger than theoretically expected decrease in ^{10}Be concentrations in
418 the upper 30 cm point to a complex post-depositional history of the alluviated pediment at Laingsburg. The deviation can be
419 explained by a first phase of low denudation rates (0.6 m/My) followed by a second phase of aeolian deflation of the surface
420 whereby finer material is preferentially removed.

421 Deflation has been reported for (semi-)arid environments during the Cenozoic (Binnie et al. 2020). The impact of deflation on
422 ^{10}Be concentrations has been described for glacial outwash terraces (Hein et al. 2009; Darvill et al. 2015) where aeolian
423 deflation and bio- or cryoturbation caused previously buried cobbles to become exposed. It has also been recorded for
424 periglacial areas of central Europe where depth profiles indicate denudation rates of 40 to 80 mMy^{-1} during the Quaternary
425 (Ruszkiczay-Rudiger et al. 2011). Binnie et al. (2020) showed that deflation on marine terraces in Northern Chile is the primary
426 cause for multimodal distributions of ^{10}Be concentration depth profiles.

427 Although the climate in southern South Africa has become more arid since the Cenozoic, the impact of aeolian deflation on
428 ^{10}Be concentrations of pediment surfaces has not yet been addressed. The results from the ^{10}Be concentration depth profile
429 indicate that caution should be taken when collecting only surface samples from alluvial pediment surfaces: boulders
430 armouring the surface of alluvial pediments can be enriched in ^{10}Be concentrations, compared to the sandy matrix, as they are
431 residual features. Based on the complex ^{10}Be concentration depth profile in the Laingsburg pediment, CRN-based denudation



432 rates from boulders could underestimate recent phases of surface deflation. Further work is needed to understand if this
433 behaviour is apparent across other pediment surfaces in the area, and how common this feature is across other pediment
434 surfaces. Future work should include concentration depth profiles from other alluvial pediments to ascertain if surface deflation
435 is occurring, and to account for this process when establishing regional long-term denudation rates from CRN.

436 **5.3 Geomorphic, tectonic, climatic and stratigraphic considerations**

437 The cosmogenic data presented in Table 3 and Fig. 9 is within the range of data presented in Fig. 3 (van der Wateren and
438 Dunai, 2001; Bierman et al., 2014; Kounov et al., 2015). There is no systematic spatial variation in surface lowering rates of
439 the pediments that can be correlated to pediment size, or geology. The Prince Albert area alluviated pediment is the most
440 isolated from the CFB, with no duricrust present (Fig. 4a), which can explain why the surface lowering rates are the highest in
441 this location (0.954 m My^{-1} compared to a maximum of 0.587 m My^{-1} for the other pediments). Further, the pediment surfaces
442 only remain fossilised as long as the duricrust remains. When the duricrust is removed denudation rates likely increase slightly
443 as shown by the Prince Albert area alluviated pediment, but will still remain low compared to other landforms (Fig. 3, Table
444 3). Therefore, the duricrusts represent an intrinsic geomorphic threshold. The ^{10}Be -derived exposure ages of the pediments are
445 *minimum* estimates, and they reveal that the pediments are older than the Pleistocene, however, to further constrain this,
446 geomorphic and stratigraphic information needs to be integrated.

447

448 The volume of material removed by river incision into the pediment surfaces equates to a lithological thickness of 42 to 141
449 m (Table 4). Assuming an average maximum denudation rate of the surrounding CFB area (10.16 m My^{-1} from Scharf et al.,
450 2013 and Kounov et al., 2015), we can estimate that the dissection started as early as ~ 2 to 14 Ma ago. Cosmogenic and
451 thermochronological (apatite fission track and (U-Th)/He) studies have reported low denudation rates across the Cenozoic,
452 and Scharf et al. (2013) stated that the close agreement between the CRN-based denudation and AFTA/(U-Th)/He exhumation
453 rates is indicative of relative tectonic stability over the last 10^6 to 10^8 years.

454

455 As the dissection would have occurred after the formation of the alluviated pediments, they need to be older than the start of
456 the incision phase (2- 14 My). Based on the observed denudation of the sub-catchments within the CFB that back the pediments
457 and the mean maximum denudation rates from Scharf et al. 2013 and Kounov et al. 2015 (Figs. 3 and 8, Table 5), we obtain
458 indicative ages of 9 - 14 My for the Laingsburg area pediment, 3 - 4 My for Floriskraal, 2 - 10 My for Leeuwgat and 2 - 28
459 My for Prince Albert. The CFB subcatchment denudation ages represent the ages of the dissecting rivers reaching the CFB
460 after dissecting the pediment surfaces. These indicative ages must be taken with caution as maximum published rates have
461 been used, and denudation rates vary over time, with a phase of increased erosion likely forming the incised channels.
462 Nonetheless, the indicative ages are useful to put the *minimum* exposure ages from cosmogenic dating in context. Furthermore,
463 as shown by the pediments causing the deflection of surrounding rivers (Fig. 13), denudation of the pediment material is
464 complicated further as the resistance of the pediment is higher than the surrounding bedrock in some locations.



465

466 Using a combination of the data above, including data on the dissection of the pediment and backing subcatchments eroded
467 into the resistant Cape Fold Belt Catchments, the Laingsburg area pediment could have an age of 23 Ma; Floriskraal 8 Ma;
468 Leeuwgat 10 Ma; and Prince Albert 17 Ma. These age estimates correspond to the timing of cessation of pediment formation
469 and start of dissection, and are based on the assumption that geomorphic process rates were steady over long timescales. As
470 denudation rates vary spatially and temporally, constant rates of erosion are unlikely as increased phases of activity are often
471 related to incision of the pediments. From geomorphic evidence, it is clear that the indicative ages are an order of magnitude
472 higher than the *minimum* exposure ages obtained from in-situ produced cosmogenic nuclide concentrations. If the cosmogenic
473 *minimum* exposure ages are used, with the volume eroded recorded using the DEM, erosion rates range from 28 to 503 m Ma⁻¹
474 which further indicates the minimum exposure ages should be taken with caution as these extremely high erosion rates have
475 not been recorded using published studies (Fig. 3). Previous works have classified pediment surfaces within height brackets
476 (e.g., King, 1953). However, in this study there is no correlation between pediment elevation and their geomorphic ages.

477

478 Duricrusts are found in many of the studied alluviated pediments (Summerfield, 1983; Marker et al., 2002), and this is well-
479 developed in the Laingsburg area pediment (Fig. 5). The alluviated pediments no longer have the overlying weathering material
480 preserved, and have been lowered to the iron pan layer. The depth profile suggests that deflation has occurred after the
481 development of the weathering mantle (Fig. 9), which has exposed the iron pan (laterites). The iron pan could have formed by
482 leaching from surrounding lithologies and clasts, by lateral movement due to groundwater change (Widdowson, 2007), or by
483 deep weathering of the bedrock. Deep weathering with the formation of iron pans occurs on low relief surfaces that have been
484 stable for at least a million years (Al-Subbary et al., 1998). Since the Cenozoic, South Africa has been relatively tectonically
485 quiescent (e.g., Bierman et al., 2014). In addition, a favourable climate of high annual rainfall, high humidity and high mean
486 annual temperature is required to form laterites (Widdowson, 2007). Further, higher concentrations of carbon dioxide are also
487 associated with the formation of laterites (and iron pans). Greenhouse episodes have occurred in the late Cretaceous and late
488 Palaeocene to early Eocene, leading to world-wide extensive weathering (Bardossy, 1981; Valetton, 1983).

489 Laterite development in southern South Africa is still poorly constrained. It has been argued to be late Pliocene in age (Marker
490 and Holmes, 1999) and have continued into the late Pleistocene (Marker and Holmes, 2005), being a component of the
491 Quaternary development of the Southern Cape (Marker et al., 2002). However, the Mediterranean climate (e.g., more humid)
492 of the coastal areas does not extend inland to the study location, which is expected for laterite development (Brown et al.,
493 1994; Braucher et al 1998a, b). Given the past climate and tectonic events, the iron pans probably formed during the late
494 Cretaceous greenhouse episode, which is compounded by the constrained dissection rates of the pediment surfaces (e.g.,
495 Dauteuil et al., 2015). The formation of duricrusts and iron pans would have occurred coevally with pediment formation, and
496 would have extended post-pediment formation (Helgren and Butzer, 1977; Widdowson, 2007). The presence of iron pans



497 indicates a period of geomorphic stability within the development of the landforms of at least 1 Ma, and probably much longer
498 and could have occurred during the denudation of the pediments.

499 **5.4 Sequence of events**

500 Pediment formation requires mountain range retreat, which causes the underlying lithological strata to be truncated (Figure
501 14). The *minimum* exposure ages calculated by cosmogenic nuclide dating using the boulder surface samples show remarkably
502 low denudation rates of the pediments during the last 3.8 Myr, which is related both to lithology (duricrust cappings, resistant
503 quartzite boulders; e.g., Scharf et al., 2013) and structure of the CFB deflecting incising rivers. The complex concentration
504 depth profile indicates that a recent phase of deflation has occurred, as there exists a discrepancy between the CRN
505 concentration of the residual boulders at the surface, and the boulders that are embedded in a sandy matrix at 30 cm depth. It
506 is important to integrate geomorphologic and stratigraphic knowledge when reporting cosmogenic nuclide results, especially
507 in an ancient setting with low denudation rates where the nuclide concentrations may reach secular equilibrium to further
508 extend the landscape development history.

509 During the Cretaceous the Cape Fold Belt was exhumed (Fig. 14; Tinker et al. 2008a, Tankard et al. 2009). During this time,
510 the folded strata was eroded and planed by hillslope processes (e.g., Rich, 1935; Bourne and Twidale, 1998), depositing
511 colluvial material and then forming soils (Fig. 14) on the alluviated pediments. This was aided by the humid climate and
512 greenhouse conditions of the Cretaceous causing deep weathering (Bardossy, 1981; Valetton, 1983). Tectonic stability allowed
513 the formation of iron pans and duricrusts, which are now exposed at the surface of the alluviated pediments due to surface
514 deflation and the removal of overbank material, as shown by the depth profile (Fig. 14). The initial planation and colluvial
515 build-up had to have occurred pre-Miocene as shown by the dissection data (Tables 4, 5). However, we posit the surfaces could
516 have formed much earlier due to the very slow processes associated with pediment formation (e.g., Lustig, 1969; Dohrenwend
517 and Parsons, 2009). By the mid-Miocene, dissection of the pediments and backing Cape Fold Belt occurred with the
518 development of small streams and subcatchments draining the pediments, with a shift towards a more fluvial dominated regime.
519 This latter stage of landscape development has decoupled the pediments from the CFB sediment source, and essentially
520 fossilised the landform (Table 3), with very low surface lowering (~0.6 m/My) and a more recent phase of aeolian deflation.

521 **5.5 Implications for landscape development**

522 The evolution of the pediment surfaces studied in South Africa indicate that the relative importance of hillslope and fluvial
523 processes (including valley development) varies over time. Therefore, the model proposed here does not fit into the previously
524 published model types (Fig. 1) that argued pediment evolution is dominated by a single process (e.g., ‘Model 1’ Figure 1;
525 Gilbert, 1877; Paige, 1912; Howard 1942 and ‘Model 2’ Fig. 1; Lawson, 1915; Rich; 1935; Kesel, 1977; Bourne and Twidale,
526 1998; Dauteuil et al., 2015), dominance varies due to lithology (e.g., ‘Model 3’ Figure 1: Lustig, 1969; Parsons and Abrahams,
527 1984) or is assisted by valley / basin development (e.g., ‘Model 4’ Fig. 1; Lustig, 1969; Parsons and Abrahams, 1984). The



528 change from hillslope to fluvial processes is likely a response to tectonic or climatic perturbations (Fig. 14). The initial
529 formation of the pediments was most likely aided by large-scale erosion during the Cretaceous (e.g., Tinker et al., 2008a,b;
530 Wildman et al., 2015, 2016; Richardson et al., 2017) and tropical conditions (Partridge and Maud, 2000).

531 The indicative geomorphic ages reported here, related to the second phase of development and the dissection of the pediments
532 by small tributaries, roughly correlate to the proposed uplift in the Cenozoic (Green et al., 2016) of 30 Ma (Burke, 1996), 18
533 Ma (Partridge and Maud, 1987) and 2.5 Ma (Partridge and Maud, 1987), and could indicate that the pediments were dissected
534 due to different pulses of uplift. Nonetheless, this time period also corresponds to variation in climate, including periods of
535 humidity reported to have ended at 30 Ma (Burke, 1996) or 18 Ma (Burke, 1996). It is not possible to distinguish the main
536 driver of dissection, and tectonic signatures are not identified within the Gouritz catchment morphometry (Richardson et al.,
537 2016).

538 The grading of the pediments indicates the main trunk rivers were active before the pediments, at least by the Miocene and
539 probably established within the Cretaceous, when large scale exhumation occurred within South Africa (e.g., Tinker et al.
540 2008a, Richardson et al., 2017). The individual grading of the pediment surfaces indicates the pediments are relatively local
541 features that react to surrounding tectonic, geological, and geomorphological settings, and are not singular surfaces (King,
542 1953). The surface lowering rates of the pediments indicate a period of low geomorphic activity as documented by other
543 researchers (Fig. 3, and references therein). There has been a drastic reduction in denudation rates since the Cretaceous as
544 shown by apatite fission track and cosmogenic nuclide studies (Fig. 3 and references therein). The data reported in this study
545 are some of the lowest in the world (Portenga and Bierman, 2011). Surface lowering is not consistent across landforms within
546 southern South Africa. Rivers are dissecting at a faster rate (Scharf et al., 2013; Kounov et al., 2015) than the pediment surfaces
547 (this study, van der Wateran and Dunai, 2001; Bierman et al., 2014; Kounov et al., 2015), which indicates that relief is
548 developing at a slow rate, as also reported by Bierman et al. (2014) from the Eastern Cape. The offshore depositional record
549 (Tinker et al. 2008a) mirrors the reduction in denudation rates with peaks in the Cenozoic most likely related to the rejuvenation
550 of the landscape, which dissected the pediments in this study (e.g., Hirsch et al., 2010; Dalton et al., 2015; Sonibare et al.,
551 2015). These increases in offshore sediment flux are minor in comparison to rates in the Cretaceous.

552 **6. Conclusion**

553 Large-scale erosional surfaces characterise the ancient landscape of southern South Africa. Cosmogenic nuclide dating using
554 ^{10}Be of four pediment surfaces in the Western Cape, and a depth profile indicate low surface lowering rates (0.315 to 0.954 m
555 My^{-1}) and *minimum* exposure ages from the Early Pleistocene. Given that the isotope concentrations are close to isotopic steady
556 state, the ^{10}Be -derived exposure ages are *minimum* estimates. Cosmogenic radionuclide depth profiling revealed that the post-
557 depositional history of the alluviated pediments is likely to be complex, with a long period of slow denudation that is followed
558 by a phase of aeolian deflation. Further work, beyond the scope of this study is needed to understand if this is a widespread



559 and characteristic feature of alluviated pediment surfaces in (semi-)arid climatic conditions. The pediments studied must be at
560 least Miocene in age, and probably much older (i.e. Cretaceous) based on the volumes of post-pediment dissection, published
561 erosion rates, the presence of duricrusts and the current understanding of tectonic and climatic variation in the region. The
562 duricrusts represent an internal geomorphic threshold which limits the rate of denudation. The dissection of the pediments has
563 been largely controlled by the structure of the Cape Fold Belt, with the initial geomorphic pulse of incision most likely related
564 to tectonic uplift or climate change. The pediments grade to individual base levels (trunk rivers), and although locally extensive,
565 they are not a regional feature representing one single surface. The presence of the pediments deflected dissecting rivers in
566 some locations and controlled landscape evolution of the surrounding rivers.

567 The pediments in southern South Africa are lowering at very low rates and are now decoupled from the surrounding rivers.
568 Therefore, they are a fossilised landform that represents a relatively stable store of sediment in which surface lowering occurs
569 by aeolian erosion causing deflation. The persistence of the pediments is due to the resistant duricrust capping and quartzitic
570 boulders, and the structural control of the Cape Fold Belt and pediments, deflecting dissecting rivers. We contend that
571 cosmogenic nuclide results must not be viewed in isolation and should be assessed together with surrounding geomorphologic
572 and stratigraphic conditions.

573 **Author Contributions**

574 Janet C. Richardson, David Hodgson and Andreas Lang collected the data. Processing and analysis of the data was completed
575 by Janet C. Richardson and Veerle Vanacker. Marcus Christl measured the $^{10}\text{Be}/^9\text{Be}$ using an accelerator mass spectrometer
576 on the 500 kV Tandy facility at ETH Zürich. Veerle Vanacker provided further support processing the data with regards to the
577 depth profile, creating Figure 9 and writing the methodology for cosmogenic nuclides. Janet C. Richardson led the writing and
578 drafting of figures, with contributions on the text and figures by Veerle Vanacker, David Hodgson and Andreas Lang.

579 **Acknowledgements**

580 The British Geomorphology Society (BSG) and British Sedimentology Research Group (BSRG) are thanked for providing
581 postgraduate grants to J. Richardson for completing this research. Jérôme Schoonejans and Marco Bravin are thanked for their
582 help during laboratory work undertaken in Université catholique de Louvain, Belgium. David Lee is thanked for his help in
583 improving Fig. 1. The landowners in South Africa are thanked for their permission to enter their land and take samples. The
584 Council of Geoscience are thanked for providing Geology GIS tiles, under the Academic/Research license. Alexandre Kounov
585 and an anonymous reviewer are thanked for their reviews of a previous version of this paper.

586



587 **Competing interests**

588 Andreas Lang is a member of the editorial board for Earth Surface Dynamics.

589 **References**

- 590 Abdelkareem, M., Ghoneim, E., El-Baz, F., and Askalany, M.: New insight on paleoriver development in the Nile basin of the
591 eastern Sahara. *J. of Afr. Ear. Sci.*, 62, 35-40, doi: 10.1016/j.jafrearsci.2011.09.001, 2012.
- 592 Aguilar, G., Riquelme, R., Martinod, J., Darrozes, J. and Maire, E.: Variability in erosion rates related to the state of landscape
593 transience in the semi-arid Chilean Andes. *ESPL*, 36, 1736-1748, doi: 10.1002/esp.2194, 2011.
- 594 Al-Subbary, A.K., Nichols, G.J., Bosence, D.W.J. and Al-Kadasi, M.: Pre-rift doming, peneplanation or subsidence in the
595 southern Red Sea? Evidence from the Medj-Zir Formation (Tawilah Group) of western Yemen. In: Purser BH, Bosence D.
596 (eds.) *Sedimentation and Tectonics in Rift Basins Red Sea:-Gulf of Aden*. Springer Netherlands. pp. 119-134, 1998
- 597 Balco, G., Stone, J.O., Lifton, N.A. and Dunai, T.J.: A complete and easily accessible means of calculating surface exposure
598 ages or erosion rates from 10 Be and 26 Al measurements. *Q. Geochron.*, 3: 174-195, doi: 10.1016/j.quageo.2007.12.001,
599 2008.
- 600 Bardossy, G.: Paleoenvironments of laterites and lateritic bauxites – effect of global tectonism on bauxite formation. In:
601 *International Seminar on Lateritisation Processes (Trivandrum, India)*. Rotterdam: Balkema, pp. 284–297, 1981
- 602 Bellin N, Vanacker V, Kubik PW. Denudation rates and tectonic geomorphology of the Spanish Betic Cordillera. *EPSL*, 390:
603 19-30, doi: 10.1016/j.epsl.2013.12.045, 2014.
- 604 Bessin, P., Guillocheau, F., Robin, C., Schrötter, J.M., Bauer, H.: Planation surfaces of the Armorican Massif (western France):
605 Denudation chronology of a Mesozoic land surface twice exhumed in response to relative crustal movements between Iberia
606 and Eurasia. *Geomorph.*, 233: 75-91, doi: 10.1016/j.geomorph.2014.09.026, 2015.
- 607 Bierman, P.R. and Caffee, M.: Slow rates of rock surface erosion and sediment production across the Namib Desert and
608 escarpment, southern Africa. *Am. J. Sci.*, 301, 326-358, 2001.
- 609 Bierman, P.R., Coppersmith, R., Hanson, K., Neveling, J., Portenga, E.W. and Rood, D.H.: A cosmogenic view of erosion,
610 relief generation, and the age of faulting in southern Africa. *GSA Today*, 24: 4-11, doi: 10.1130/GSATG206A.1, 2014.
- 611 Binnie, A., Binnie, S.A., Parteli, E.J.R. and Dunai, T.J.: The implications of sampling approach and geomorphological
612 processes for cosmogenic 10Be exposure dating of marine terraces. *Nucl. Instrum. and Methods Phys. Res. Sec. B*, 467, 130-
613 139, doi: 10.1016/j.nimb.2019.12.017 , 2020.
- 614 Bishop, P.: Long-term landscape evolution: linking tectonics and surface processes. *ESPL*, 32: 329-365, doi:
615 10.1002/esp.1493, 2007.
- 616 Bloom, A.L.: Teaching about relict, no-analog landscapes. *Geomorph.*, 47: 303-311, doi: 10.1016/S0169-555X(02)00094-6 ,
617 2002.



- 618 Bourne, J.A. and Twidale, C.R.: Pediments and alluvial fans: genesis and relationships in the western piedmont of the Flinders
619 Ranges, South Australia. *Aust. J. Earth Sci.*, 45: 123–135, doi: 10.1080/08120099808728373, 1998.
- 620 Braucher, R., Bourles, D.L., Colin, F., Brown, E.T. and Boulange, B.: Brazilian laterite dynamics using in situ-produced 10
621 Be. *EPSL*, 163: 197-205, doi: 10.1016/S0012-821X(98)00187-3, 1998.
- 622 Braucher R., Colin, F., Brown, E.T., Bourles, D.L., Bamba, O., Raisbeck, G.M., You, F. and Koud, J.M.: African laterite
623 dynamics using in situ-produced 10 Be. *Geochem. Cosmo. Acta*, 62, 1501-1507, doi: 10.1016/S0016-7037(98)00085-4, 1998.
- 624 Braucher, R., Brown, E.T., Bourlès, D.L. and Colin, F.: In situ produced 10 Be measurements at great depths: implications for
625 production rates by fast muons. *EPSL*, 211, 251-258, doi: 10.1016/S0012-821X(03)00205-X, 2003.
- 626 Braucher, R., Merchel, S., Borgomano, J. and Bourlès, D.L.: Production of cosmogenic radionuclides at great depth: A
627 multielement approach, *EPSL*, 309, 1–9, doi: 10.1016/j.epsl.2011.06.036 , 2011.
- 628 Braun, J., Guillocheau, F., Robin, C., Baby, G. and Jelsma, H.: Rapid erosion of the Southern African Plateau as it climbs over
629 a mantle superswell. *J. Geophys. Res.: Solid Earth*: 119, 6093-6112, doi: 10.1002/2014JB010998, 2014.
- 630 Brocklehurst, S.H. and Whipple, K.X.: Glacial erosion and relief production in the Eastern Sierra Nevada, California.
631 *Geomorph.*, 42, 1–24, doi: 10.1016/S0169-555X(01)00069-1, 2002.
- 632 Brook, E.J., Brown, E.T., Kurz, M.D., Ackert, R.P., Raisbeck, G.M. and Yiou, F.: Constraints on age, erosion, and uplift of
633 Neogene glacial deposits in the Transantarctic Mountains determined from in situ cosmogenic ^{10}Be and ^{26}Al . *Geol.*, 23, 1063-
634 1066, doi: 10.1130/0091-7613(1995)023<1063:COAEAU>2.3.CO;2, 1995.
- 635 Brown, E.T., Bourlès, D.L., Colin, F., Sanfo, Z., Raisbeck, G.M., and Yiou, F.: The development of iron crust lateritic systems
636 in Burkina Faso, West Africa examined with in-situ-produced cosmogenic nuclides. *EPSL*, 124, 19-33, doi: 10.1016/0012-
637 821X(94)00087-5, 1994.
- 638 Brown, R.W., Rust, D.J., Summerfield, M.A., Gleadow, A.J. and De Wit, M.C.: An Early Cretaceous phase of accelerated
639 erosion on the south-western margin of Africa: Evidence from apatite fission track analysis and the offshore sedimentary
640 record. *Int. J. Rad. Appl. Instr. A. Part D. Nucl. Tracks and Radiat. Meas.*, 17, 339-350, doi: 10.1016/1359-0189(90)90056-
641 4, 1990.
- 642 Brown, R.W., Summerfield, M.A. and Gleadow, A.J.W.: Denudation history along a transect across the Drakensberg
643 Escarpment of southern Africa derived from apatite fission track thermochronology. *J. Geophys. Res.*, 107, 1-18, doi:
644 10.1029/2001JB000744, 2002.
- 645 Bryan, K.: Erosion and sedimentation in the Papago country, Arizona. *U.S Geol. Surv. Bull.*, 730, 19–90, 1923.
- 646 Burbank, D.W., Leland, J., Fielding, E., Anderson, R.S., Brozovic, N., Reid, M.R. and Duncan, C.: Bedrock incision, rock
647 uplift and threshold hillslopes in the northwestern Himalayas. *Nature*, 379, 505-510, 1996.
- 648 Burke, K. The African plate. *S. Afri. J. Geol.*, 99, 341-409, 1996.
- 649 Carignano, C., Cioccale, M., and Rabassa, J.: Landscape antiquity of the Central Eastern Sierras Pampeanas (Argentina):
650 Geomorphological evolution since Gondwanic times. *Z. Geomorph. Supplement Band 118*, 245–268, 1999.



- 651 Chadwick, O.A., Roering, J.J., Heimsath, A.M., Levick, S.R., Asner, G.P. and Khomo, L.: Shaping post-orogenic landscapes
652 by climate and chemical weathering. *Geol.*, 41, 1171-1174, doi: 10.1130/G34721.1, 2013.
- 653 Chappell, J., Zheng, H. and Fifield, K.: Yangtse River sediments and erosion rates from source to sink traced with cosmogenic
654 ¹⁰Be: Sediments from major rivers. *Palaeo.*, 241, 79-94, doi: 10.1016/j.palaeo.2006.06.010, 2006.
- 655 Chmeleff, J., von Blanckenburg, F., Kossert, K. and Jakob, D.: Determination of the ¹⁰Be half-life by multicollector ICP-MS
656 and liquid scintillation counting. *Nucl. Instrum. and Methods in Phys. Res. B*, 263, 192–199, doi: 10.1016/j.nimb.2009.09.012,
657 2010.
- 658 Chorley, R.J., Schumm, S.A. and Sugden, D.E.: *Geomorphology*, London. Methuen and Co. 648 pp, 1984.
- 659 Christl, M., Vockenhuber, C., Kubik, P.W., Wacker, L., Lachner, J., Alfimov, V. and Synal, H.-A.: The ETH Zurich AMS
660 facilities: Performance parameters and reference materials. *Nucl. Instrum. and Methods in Phys. Res. B*, 294, 29-38, doi:
661 10.1016/j.nimb.2012.03.004, 2-13, 2013.
- 662 Cockburn, H.A.P., Brown, R.W., Summerfield, M.A. and Seidl, M.A.: Quantifying passive margin denudation and landscape
663 development using a combined fission-track thermochronology and cosmogenic isotope analysis approach. *EPSL*, 179, 429-
664 435, doi: 10.1016/S0012-821X(00)00144-8, 2000.
- 665 Codilean, A.T., Bishop, P., Stuart, F.M., Hoey, T.B., Fabel, D. and Freeman, S.P.: Single-grain cosmogenic ²¹Ne
666 concentrations in fluvial sediments reveal spatially variable erosion rates. *Geol.*, 36, 159-162, doi: 10.1130/G24360A.1, 2008.
- 667 Dalton, T.J.S., Paton, D.A., Needham, T. and Hodgson, N.: Temporal and spatial evolution of deepwater fold thrust belts:
668 Implications for quantifying strain imbalance. *Interpret.*, 3, SAA59-SAA70, doi: 10.1190/INT-2015-0034.1, 2015.
- 669 Darvill, C.M., Bentley, M.J., Stokes, C.R., Hein, A.S. and Rodés, Á.: Extensive MIS 3 glaciation in southernmost Patagonia
670 revealed by cosmogenic nuclide dating of outwash sediments. *EPSL*, 429, 157-169, doi: 10.1016/j.epsl.2015.07.030, 2015.
- 671 Dauteuil, O., Bessin, P. and Guillocheau, F.: Topographic growth around the Orange River valley, southern Africa: A Cenozoic
672 record of crustal deformation and climatic change. *Geomorph.*, 233, 5-19, doi: 10.1016/j.geomorph.2014.11.017, 2015.
- 673 Davis, W.M. Observations in South Africa. *Geol. Soc. Am. Bull.*, 17, 377-450, 1906.
- 674 Dean, W.R.J., Hoffinan, M.T., Meadows, M.E. and Milton, S.J.: Desertification in the semi-arid Karoo, South Africa: review
675 and reassessment. *J. Arid Env.*, 30, 247-264, doi: 10.1016/S0140-1963(05)80001-1, 1995.
- 676 Decker, J.E., Niedermann, S. and de Wit, M.J.: Soil erosion rates in South Africa compared with cosmogenic ³He-based rates
677 of soil production. *S. Afri. J. Geol.*, 114, 475-488, doi: 10.2113/gssajg.114.3-4.475, 2011.
- 678 Decker, J.E., Niedermann S. and de Wit, M.J.: Climatically influenced denudation rates of the southern African plateau: Clues
679 to solving a geomorphic paradox. *Geomorph.*, 190, 48-60, doi: 10.1016/j.geomorph.2013.02.007, 2013.
- 680 Doucouré, C.M. and de Wit, M.J.: Old inherited origin for the present near-bimodal topography of Africa. *J. Afr. Earth Sci.*,
681 36, 371-388, doi: doi.org/10.1016/S0899-5362(03)00019-8, 2003
- 682 Demoulin, A., Zárata, M. and Rabassa, J.: Long-term landscape development: a perspective from the southern Buenos Aires
683 ranges of east central Argentina. *J. S Am. Earth Sci.*, 19, 193–204, doi: 10.1016/j.jsames.2004.12.001, 2005.



- 684 De Smith, M.J., Goodchild, M.F. and Longley, P.: Geospatial analysis: a comprehensive guide to principles, techniques and
685 software tools. Troubador Publishing Ltd. pp. 389, 2007.
- 686 de Wit M.: The Kalahari Epeirogeny and climate change: differentiating cause and effect from core to space. *S. Afri. J. Geol.*,
687 110, 367-392, doi: 10.2113/gssajg.110.2-3.367, 2007.
- 688 Dirks, P.H., Kibii, J.M., Kuhn, B.F., Steininger, C., Churchill, S.E., Kramers, J.D., Pickering, R., Farber, D.L., Mériaux, A.S.,
689 Herries, A.I. and King G.C. Geological setting and age of Australopithecus sediba from southern Africa. *Sci*, 328, 205-208,
690 doi: 10.1126/science.1184950, 2010.
- 691 Dixey, F.: African landscape. *Geograph. Rev.*, 34, 457-465, doi: 10.2307/209976, 1944.
- 692 Dohrenwend, J.C. and Parsons, A.J.: Pediments in arid environments. In: Abrahams, A.D., Parsons, A.J. (Eds.)
693 *Geomorphology of desert environments*. Springer Netherlands. pp. 377-411, 2009.
- 694 Doucouré CM, de Wit MJ. 2003. Old inherited origin for the present near bimodal topography of Africa. *J. Afri. Earth Sci.*,
695 36, 371–388, doi: 10.1016/S0899-5362(03)00019-8, 2003.
- 696 Dunai, T.J.: Scaling factors for production rates of in situ produced cosmogenic nuclides: a critical reevaluation, *EPSL*, 176,
697 157-169, doi: 10.1016/S0012-821X(99)00310-6, 2000.
- 698 Dunai TJ. 2010. *Cosmogenic Nuclides: Principles, Concepts and Applications in the Earth Surface Sciences*, Cambridge
699 University Press, Cambridge, UK, 2010.
- 700 Dunai, T.J., López, G.A.G. and Juez-Larré, J.: Oligocene–Miocene age of aridity in the Atacama Desert revealed by exposure
701 dating of erosion-sensitive landforms. *Geol.*, 33, 321-324, doi: 10.1130/G21184.1, 2005.
- 702 Du Toit, A.: *Our Wandering Continents*. Oliver and Boyd, U.K, 366 pp, 1937.
- 703 Du Toit, A.: *The Geology of South Africa*, 3rd edn. Oliver and Boyd, U.K. 539 pp, 1954.
- 704 Ebinger, C.J. and Sleep, N.H.: Cenozoic magmatism throughout east Africa resulting from impact of a single plume. *Nature*,
705 395, 788-791, 1998.
- 706 Erlanger, E.D., Granger, D.E. and Gibbon, R.J.: Rock uplift rates in South Africa from isochron burial dating of fluvial and
707 marine terraces. *Geol.*, 40, 1019-1022, doi: 10.1130/G33172.1, 2012.
- 708 Fleming, A., Summerfield, M.A., Stone, J.O., Fifield, L.K. and Cresswell, R.G.: Denudation rates for the southern Drakensberg
709 escarpment, SE Africa, derived from in-situ-produced cosmogenic ³⁶Cl: initial results. *J. Geol. Soc.*, 156, 209-212, doi:
710 10.1144/gsjgs.156.2.0209, 1999.
- 711 Flowers, R.M. and Schoene, B.: (U-Th)/He thermochronometry constraints on unroofing of the eastern Kaapvaal craton and
712 significance for uplift of the southern African Plateau. *Geol.*, 38, 827-830, doi: doi.org/10.1130/G30980.1, 2010.
- 713 Gallagher, K. and Brown, R.: The Mesozoic denudation history of the Atlantic margins of southern Africa and southeast Brazil
714 and the relationship to offshore sedimentation. *Geol. Soc., London, Sp. Pub.*, 153, 41-53, doi: 10.1144/GSL.SP.1999.153.01.0,
715 1999.
- 716 Ghosh, P., Sinha, S. and Misra, A.: Morphometric properties of the trans-Himalayan river catchments: Clues towards a relative
717 chronology of orogen-wide drainage integration. *Geomorph.*, 233, 127-141, doi: 10.1016/j.geomorph.2014.10.035, 2014.



- 718 Gilbert, G.K.: Report on the geology of the Henry Mountains. US Geographical and Geological Survey of the Rocky Mountain
719 Region. Washington, DC: U.S. Department of the Interior, 1877.
- 720 Gorelov, S.K., Drenev, N.V., Mescheryakov Y.A., Tikanov, N.A. and Fridland, V.M.: Planation surfaces of the USSR.
721 Geomorph., 1, 18–29, 1970.
- 722 Granger, D.E., Kirchner, J.W. and Finkel, R.C.: Quaternary downcutting rate of the New River, Virginia, measured from
723 differential decay of cosmogenic ²⁶Al and ¹⁰Be in cave-deposited alluvium. *Geol.*, 25, 107-110, doi: 10.1130/0091-
724 7613(1997)025<0107:QDROTN>2.3.CO;2, 1997.
- 725 Green, P.F., Duddy, I.R., Japsen P., Bonow, J.M. and Malan, J.A.: Post-breakup burial and exhumation of the southern margin
726 of Africa. *Basin Res.*, 29, 96 – 127, doi: 10.1111/bre.12167, 2016.
- 727 Guillocheau, F., Chelalou, R., Linol, B., Dauteuil, O., Robin, C., Mvondo, F., Callec, Y. and Colin, J.P.: Cenozoic landscape
728 evolution in and around the Congo Basin: constraints from sediments and planation surfaces. In: de Wit, M.J., Guillocheau, F.
729 and de Wit, M.C.J. (eds) *Geology and Resource Potential of the Congo Basin. Regional Geology Reviews*, Springer, 271-313,
730 2015.
- 731 Guillocheau, F., Simon, B., Baby, G., Bessin, P., Robin, C. and Dauteuil, O.: Planation surfaces as a record of mantle dynamics:
732 the case example of Africa. *Gondwana Res.*, 53, 82-98, doi: 10.1016/j.gr.2017.05.015, 2018.
- 733 Gunnell, Y., Braucher, R., Bourles, D. and André, G.: Quantitative and qualitative insights into bedrock landform erosion on
734 the South Indian craton using cosmogenic nuclides and apatite fission tracks. *Geol. Soc. Am. Bull.*, 119, 576-585, doi:
735 10.1130/B25945.1, 2007.
- 736 Hagedorn, J.: Silcretes in the Western Little Karoo and their relation to geomorphology and palaeoecology: *Palaeoecol. of*
737 *Afr.*, 19, 371–375, 1988.
- 738 Helgren, D.M. and Butzer, K.W.: Paleosols of the southern Cape Coast, South Africa: implications for laterite definition,
739 genesis, and age. *Geograph. Rev.*, 67, 430-445, doi: 10.2307/213626, 1977.
- 740 Hein, A.S., Hulton, N.R., Dunai, T.J., Schnabel, C., Kaplan, M.R., Naylor, M. and Xu, S.: Middle Pleistocene glaciation in
741 Patagonia dated by cosmogenic-nuclide measurements on outwash gravels. *EPSL*, 286, 184-197, doi:
742 10.1016/j.epsl.2009.06.026, 2009.
- 743 Hirsch, K.K., Scheck-Wenderoth, M., van Wees, J.D., Kuhlmann, G. and Paton, D.A.: Tectonic subsidence history and thermal
744 evolution of the Orange Basin. *Mar. Petrol. Geol.*, 27, 565-584, doi: 10.1016/j.marpetgeo.2009.06.009, 2010.
- 745 Howard, A.D. 1942. Pediment passes and the pediment problem. US Coast and Geodetic Survey, 1942.
- 746 Jackson J., Ritz, J.F., Siame, L., Raisbeck, G., Yiou, F., Norris, R., Youngson, J. and Bennett, E.: Fault growth and landscape
747 development rates in Otago, New Zealand, using in situ cosmogenic ¹⁰ Be. *EPSL*, 195, 185-193, doi: 10.1016/S0012-
748 821X(01)00583-0, 2002.
- 749 Jerolmack, D.J., Paola, C.: Shredding of environmental signals by sediment transport. *Geophys. Res. Lett.*, 37, L19401., doi:
750 10.1029/2010GL044638, 2010.
- 751 Kesel, R.H.: Some aspects of the geomorphology of inselbergs in central Arizona, USA. *Z. Geomorph.*, 21, 119–46, 1977.



- 752 Keen-Zebert, A., Tooth, S. and Stuart, F.M.: Cosmogenic ^3He measurements provide insight into lithologic controls on
753 bedrock channel incision: examples from the South African interior. *J. Geol.*, 124, 423-434, doi: 10.1086/685506, 2016.
- 754 King, L.C.: On the ages of African land-surfaces. *Quart. J. Geol. Soc.*, 104: 439-45, doi: 10.1144/GSL.JGS.1948.104.01-04.20,
755 1948.
- 756 King, L.C.: The pediment landform: some current problems. *Geol. Mag.*, 86, 245-250, doi: 10.1017/S0016756800074665,
757 1949.
- 758 King, L.C.: The geology of the Makapan and other caves. *Trans. Royal Soc. S. Afr.*, 33: 121-151, doi:
759 10.1080/00359195109519881, 1951.
- 760 King, L.C.: Canons of landscape evolution. *Geol. Soc. Am. Bull.*, 64, 721-752, doi: 10.1130/0016-
761 7606(1953)64[721:COLE]2.0.CO;2, 1953.
- 762 King, L.C.: Pediplanation and isostasy: an example from South Africa. *Quart. J. Geol. Soc.*, 111, 353-359, doi:
763 10.1144/GSL.JGS.1955.111.01-04.18, 1955.
- 764 King, L.C. 1956a. A geomorphological comparison between Eastern Brazil and Africa (Central and Southern). *Quart. J. Geol.*
765 *Soc.*, 112, 445–474, doi: 10.1144/GSL.JGS.1956.112.01-04.2, 1956a.
- 766 King, L.C. 1956b. A geomorfologia do Brasil oriental. *Rev. Bras. Geog.* 18,186–263, 1956b.
- 767 King, L.C. South African scenery. A textbook of geomorphology. 308 pp, 1963.
- 768 Kounov, A., Niedermann, S., de Wit, M.J., Viola, G., Andreoli, M. and Erzinger, J.: Present denudation rates at selected
769 sections of the South African escarpment and the elevated continental interior based on cosmogenic ^3He and ^{21}Ne . *S. Afr. J.*
770 *Geol.* 110, 235-248, doi: 10.2113/gssajg.110.2-3.235, 2007.
- 771 Kounov, A., Viola, G., De Wit, M. and Andreoli, M.A.G.: Denudation along the Atlantic passive margin: new insights from
772 apatite fission-track analysis on the western coast of South Africa. *Geol. Soc. London, Sp. Pub.*: 324, 287-306, doi:
773 10.1144/SP324.19, 2009.
- 774 Kounov, A., Niedermann, S., de Wit, M.J., Codilean, A.T., Viola, G., Andreoli, M. and Christl, M.: Cosmogenic ^{21}Ne and
775 ^{10}Be reveal a more than 2 Ma Alluvial Fan Flanking the Cape Mountains, South Africa. *S. Afr. J. Geol.*, 118, 129-144, doi:
776 10.2113/gssajg.118.2.129, 2015.
- 777 Kubik, P.W. and Christl, M.: ^{10}Be and ^{26}Al measurements at the Zurich 6 MV Tandem AMS facility. *Nucl. Instrum. Methods*
778 *in Phys. Res. Section B*, 268, 880–883, doi: 10.1016/j.nimb.2009.10.054, 2010.
- 779 Lawson, A.C.: The epigene profiles of the desert. *Uni. California Dept. Geol. Bull.*, 9, 23–48, 1915.
- 780 Lidmar-Bergström, K.: Exhumed cretaceous landforms in south Sweden. *Z. Geomorph.: Supp. Band 72*, 21–40, 1988.
- 781 Lustig, L.K.: Trend surface analysis of the Basin and Range province, and some geomorphic implications. *US Geol. Surv.*
782 *Profess. Paper 500-D*, 1969.
- 783 Marker, M.E. and Holmes, P.J.: Laterisation on limestones of the Tertiary Wankoe Formation and its relationship to the African
784 Surface, southern Cape, South Africa. *Catena*, 38, 1-21, doi: 10.1016/S0341-8162(99)00066-1, 1999.



- 785 Marker ME, Holmes PJ. 2005. Landscape evolution and landscape sensitivity: the case of the southern Cape. South African
786 Journal of Science: 101, 53 - 60.
- 787 Marker, M.E., McFarlane, M.J. and Wormald, R.J.: A laterite profile near Albertinia, Southern Cape, South Africa: its
788 significance in the evolution of the African Surface. S. Afr. J. Geol., 105, 67-74, doi: 10.2113/1050067, 2002.
- 789 Margerison, H.R., Phillips, W.M., Stuart, F.M. and Sugden, D.E.: Cosmogenic ³He concentrations in ancient flood deposits
790 from the Coombs Hills, northern Dry Valleys, East Antarctica: interpreting exposure ages and erosion rates. EPSL, 230, 163-
791 175, doi: 10.1016/j.epsl.2004.11.007, 2005.
- 792 Midgley, G.F., Hannah, L., Millar, D., Thuiller, W. and Booth, A.: Developing regional and species-level assessments of
793 climate change impacts on biodiversity in the Cape Floristic Region. Bio. Cons., 112, 87-97, doi: 10.1016/S0006-
794 3207(02)00414-7, 2003.
- 795 Moore, A., Blenkinsop, T. and Cotterill, F.W.: Southern African topography and erosion history: plumes or plate tectonics?
796 Terra Nova: 21, 310-315, doi: 10.1111/j.1365-3121.2009.00887.x, 2009.
- 797 Mountain, E.D: Grahamstown peneplain. Trans. Geol. Soc. S Afr., 83, 47-53, 1980.
- 798 Norton, K.P. and Vanacker, V.: Effects of terrain smoothing on topographic shielding correction factors for cosmogenic
799 nuclide-derived estimates of basin-averaged denudation rates. ESPL, 34, 145-154, doi: 10.1002/esp.1700, 2009.
- 800 Nyblade, A.A. and Robinson, S.W.: The african superswell. Geophys. Res. Lett., 21, 765-768, doi: 10.1029/94GL00631, 1994.
- 801 Ollier, C.: Ancient landscapes. Belhaven Press, London/New York, 233 pp, 1991.
- 802 Ollier, C. and Pain, C.: The origin of mountains. Routledge, London/New York, 345 pp, 2000.
- 803 Ouimet, W.B., Whipple, K.X., Crosby, B.T., Johnson, J.P. and Schildgen, T.F.: Epigenetic gorges in fluvial landscapes. ESPL,
804 33, 1993-2009, doi: 10.1002/esp.1650, 2008.
- 805 Owen, L.A., Finkel, R.C., Barnard, P.L., Haizhou, M., Asahi, K., Caffee, M.W. and Derbyshire, E.: Climatic and topographic
806 controls on the style and timing of Late Quaternary glaciation throughout Tibet and the Himalaya defined by ¹⁰Be cosmogenic
807 radionuclide surface exposure dating. Quat. Sci. Rev., 24, 1391-1411, doi: 10.1016/j.quascirev.2004.10.014, 2005.
- 808 Paige, S.: Rock-cut surfaces in the desert regions. J. Geol., 20, 442-50, 1912.
- 809 Panario, D., Gutiérrez, O., Sánchez Bettucci, L., Peel, E., Oyhantçabal, P., Rabassa, J.: Ancient landscapes of Uruguay. In:
810 Rabassa, J. and Ollier, C. (Eds.) Gondwana landscapes in southern South America, pp. 161-199, 2014.
- 811 Parsons, A.J. and Abrahams, A.D.: Mountain mass denudation and piedmont formation in the Mojave and Sonoran Deserts.
812 Am. J. Sci., 284, 255-71, 1984.
- 813 Partridge, T.C.: Cainozoic environmental change in southern Africa, with special emphasis on the last 200 000 years. Prog.
814 Phys. Geog., 21, 3-22, doi: 10.1177/030913339702100102, 1997.
- 815 Partridge, T.C. 1998. Of diamonds, dinosaurs and diastrophism: 150 million years of landscape evolution in southern Africa.
816 South African Journal of Geology: 101, 165-184.
- 817 Partridge, T.C.: Evolution of Landscapes. In: Cowling, R.M., Richardson, D.M. and Pierce, S.M. (eds). Vegetation of southern
818 Africa. Cambridge University Press, pp. 1-20, 1999.



- 819 Partridge, T.C. and Maud, R.R.: Geomorphic evolution of southern Africa since the Mesozoic. *S. Afr. J. of Geol.*, 90, 179-
820 208, 1987.
- 821 Partridge, T.C. and Maud, R.R. Macro-scale geomorphic evolution of southern Africa. In Partridge T.C. and Maud, R.R.M.
822 (eds) *The Cenozoic of southern Africa*. Oxford University Press. pp. 3 – 18, 2000.
- 823 Paton, D.A.: Influence of crustal heterogeneity on normal fault dimensions and evolution: southern South Africa extensional
824 system. *J. Struct. Geol.*, 28, 868-886, doi: 10.1016/j.jsg.2006.01.006, 2006.
- 825 Peulvast, J.P. and Bétard F.: A history of basin inversion, scarp retreat and shallow denudation: The Araripe basin as a keystone
826 for understanding long-term landscape evolution in NE Brazil. *Geomorph.*, 233, 20-40, doi: 10.1016/j.geomorph.2014.10.009,
827 2015.
- 828 Portenga, E.W. and Bierman, P.R.: Understanding Earth's eroding surface with ¹⁰Be. *GSA Today*: 21, 4-10, doi:
829 10.1130/G111A.1, 2011.
- 830 Rich, J.L.: Origin and evolution of rock fans and pediments. *Bull. Geol. Soc. Am.*, 46, 999–1024, doi: 10.1130/GSAB-46-999,
831 2935, 1935.
- 832 Richardson, J.C., Hodgson, D.M., Wilson, A., Carrivick, J.L. and Lang A.: Testing the applicability of morphometric
833 characterisation in discordant catchments to ancient landscapes: A case study from southern Africa. *Geomorph.*, 201, 162-176,
834 doi: 10.1016/j.geomorph.2016.02.026, 2016.
- 835 Richardson, J.C., Hodgson, D.M., Paton, D., Craven, B., Rawcliffe, A. and Lang, A.: Where is my sink? Reconstruction of
836 landscape development in southwestern Africa since the Late Jurassic. *Gondwana Res.*: 45, 43-64, doi:
837 10.1016/j.gr.2017.01.004, 2017.
- 838 Rogers, C.A.: The geological history of the Gouritz River system. *Trans. S. Afri. Phil. Soc.*, 14, 375-384, 1903.
- 839 Romans, B.W., Castelltort, S., Covault, J.A., Fildani, A. and Walsh, J.P.: Environmental signal propagation in sedimentary
840 systems across timescales. *Earth-Sci. Rev.*: 153: 7-29, doi: 10.1016/j.earscirev.2015.07.012, 2016.
- 841 Ruzsiczay-Rüdiger, Z., Braucher, R., Csillag, G., Fodor, L.I., Dunai, T.J., Bada, G., Bourlés, D. and Müller, P.: Dating
842 Pleistocene aeolian landforms in Hungary, Central Europe, using in situ produced cosmogenic ¹⁰Be. *Quat. Geochron.*, 6, 515-
843 529, doi: 10.1016/j.quageo.2011.06.001, 2011.
- 844 Scharf, T.E., Codilean, A.T., de Wit, M., Jansen, J.D., Kubik, P.W.: Strong rocks sustain ancient postorogenic topography in
845 southern Africa. *Geol.*, 41, 331-334, doi: 10.1130/G33806.1, 2013.
- 846 Sharp, R.P.: Geomorphology of the Ruby–East Humboldt Range, Nevada. *Bull. Geol. Soc. Am.*, 51, 337–72, doi:
847 10.1130/GSAB-51-337, 1940.
- 848 Sømme, T.O., Piper, D.J., Deptuck, M.E. and Helland-Hansen, W.: Linking onshore–offshore sediment dispersal in the Golo
849 source-to-sink system (Corsica, France) during the Late Quaternary. *J. Sed. Res.*: 81, 118-137, doi: 10.2110/jsr.2011.11, 2011
- 850 Sonibare, W.A., Sippel, J., Scheck-Wenderoth, M. and Mikeš, D.: Crust-scale 3D model of the Western Bredasdorp Basin
851 (Southern South Africa): data-based insights from combined isostatic and 3D gravity modelling. *Basin Res.*, 27, 125-151, doi:
852 10.1111/bre.12064, 2015.



- 853 Spikings, A.L., Hodgson, D.M., Paton, D.A. and Spychala, Y.T.: Palinspastic restoration of an exhumed deep-water system:
854 a workflow to improve paleogeographic reconstructions. *Interpretation*, 3, SAA71-SAA87, doi: 10.1190/INT-2015-0015.1,
855 2015
- 856 Stanley, J.R., Braun, J., Baby, G., Guillocheau, F., Robin, C., Flowers, R.M., Brown, R., Wildman, M. and Beucher, R.:
857 Constraining plateau uplift in southern Africa by combining thermochronology, sediment flux, topography, and landscape
858 evolution modeling. *J. Geophys. Res.: Solid Earth*, 126(7), p.e2020JB021243, doi: 10.1029/2020JB021243, 2021
- 859 Summerfield, M.A.: Silcrete as a palaeoclimatic indicator: evidence from southern Africa. *Palaeo.*, *Palaeo.*, *Palaeo.*, 41, 65-
860 79, doi: 10.1016/0031-0182(83)90076-7, 1983.
- 861 Tankard, A., Welsink, H., Aukes, P., Newton, R. and Stettler, E.: Tectonic evolution of the Cape and Karoo basins of South
862 Africa. *Mar. Pet. Geol.*, 26, 1379-1412, doi: 10.1016/j.marpetgeo.2009.01.022, 2009.
- 863 Tinker, J., De Wit, M. and Brown, R.: Mesozoic exhumation of the southern Cape, South Africa, quantified using apatite
864 fission track thermochronology. *Tectonophys.*: 455, 77-93, doi: 10.1016/j.tecto.2007.10.009, 2008a.
- 865 Tinker J., de Wit, M. and Brown, R.: Linking source and sink: evaluating the balance between onshore erosion and offshore
866 sediment accumulation since Gondwana break-up, South Africa. *Tectonophys.*, 455, 94-103, doi: 10.1016/j.tecto.2007.11.040,
867 2008b.
- 868 Twidale, C.R.: *Ancient Australian Landscapes*. Rosenberg Pub Pty Limited, 144 pp, 2007a.
- 869 Twidale, C.R.: Bornhardts and associated fracture patterns. *Rev. As. Geol. Arg.*, 62, 139–153, 2007b.
- 870 Valeton, I.: Palaeoenvironment of lateritic bauxites with vertical and lateral differentiation. *Geol. Soc. London Sp. Pub.*, 11,
871 77–90, doi: 10.1144/GSL.SP.1983.011.01.10, 1983.
- 872 Vandermaelen, N., Beerten, K., Clapuyt, F., Christl, M. and Vanacker, V.: Constraining the aggradation mode of Pleistocene
873 river deposits based on cosmogenic radionuclide depth profiles and numerical modelling. *Geochron. Dis.*, 2022, 1-31, doi:
874 10.5194/gchron-4-713-2022, 2022.
- 875 Vanacker V., von Blanckenburg, F., Hewawasam, T. and Kubik, P.W.: Constraining landscape development of the Sri Lankan
876 escarpment with cosmogenic nuclides in river sediment, *EPSL*, 253, 402-414, doi: 10.1016/j.epsl.2006.11.003, 2007.
- 877 Vanacker, V., von Blanckenburg, F., Govers, G., Molina, A., Campforts, B. and Kubik, P.W.: Transient river response,
878 captured by channel steepness and its concavity. *Geomorph.*, 228, 234-243, doi: 10.1016/j.geomorph.2014.09.013, 2015.
- 879 van der Beek, P., Summerfield, M.A., Braun, J., Brown, R.W. and Fleming A.: Modeling postbreakup landscape development
880 and denudational history across the southeast African (Drakensberg Escarpment) margin. *J. Geophys. Res.: Solid Earth*: 107
881 (B12), doi: 10.1029/2001JB000744, 2002.
- 882 van der Wateren, F.M. and Dunai, T.J.: Late Neogene passive margin denudation history—cosmogenic isotope measurements
883 from the central Namib desert. *Glob. and Planet. Change*, 30, 271-307, doi: 10.1016/S0921-8181(01)00104-7, 2001.
- 884 van Niekerk, H.S., Beukes, N.J. and Gutzmer, J.: Post-Gondwana pedogenic ferromanganese deposits, ancient soil profiles,
885 African land surfaces and palaeoclimatic change on the Highveld of South Africa. *J. Afr. Earth Sci.*, 29, 761-781, doi:
886 10.1016/S0899-5362(99)00128-1, 1999.



- 887 Vermeesch, P.: CosmoCalc: An Excel add-in for cosmogenic nuclide calculations. *Geochem., Geophys., Geosyst.*: 8,
888 doi:10.1029/2006GC001530, 2007
- 889 von Blanckenburg F., Belshaw, N. and O'Nions, R.: Separation of ^9Be and cosmogenic ^{10}Be from environmental materials
890 and SIMS isotope dilution analysis. *Chem. Geol.*, 129, 93–99, doi: 10.1016/0009-2541(95)00157-3, 1996.
- 891 von Blanckenburg, F., Hewawasam, T., Kubik, P.W.: Cosmogenic nuclide evidence for low weathering and denudation in the
892 wet, tropical highlands of Sri Lanka. *J. Geophys. Res.: Earth Surface*: 109, F3, doi: 10.1029/2003JF000049, 2004.
- 893 Widdowson, M.: Laterite and Ferricrete. In: Nash DJ, McLaren SJ. (eds.) *Geochemical Sediments and Landscapes*. Oxford,
894 UK: Wiley-Blackwell, pp. 46–94, 2007.
- 895 Wildman, M., Brown, R., Watkins, R., Carter, A., Gleadow, A. and Summerfield, M.: Post break-up tectonic inversion across
896 the southwestern cape of South Africa: new insights from apatite and zircon fission track thermochronometry. *Tectonophys.*,
897 654, 30–55, doi: 10.1016/j.tecto.2015.04.012, 2015.
- 898 Wildman, M., Brown, R., Beucher, R., Persano, C., Stuart, F., Gallagher, K., Schwanethal, J. and Carter, A.: The chronology
899 and tectonic style of landscape evolution along the elevated Atlantic continental margin of South Africa resolved by joint
900 apatite fission track and (U-Th-Sm)/He thermochronology. *Tectonics*: 35, doi: 10.1002/2015TC004042, 2016.
- 901 Wildman, M., Brown, R., Persano, C., Beucher, R., Stuart, F.M., Mackintosh, V., Gallagher, K., Schwanethal, J. and Carter,
902 A.: Contrasting Mesozoic evolution across the boundary between on and off craton regions of the South African plateau
903 inferred from apatite fission track and (U-Th-Sm)/He thermochronology. *J. Geophys. Res.: Solid Earth*, 122(2), pp.1517-1547,
904 doi: 10.1002/2016JB013478, 2017.
- 905 Willenbring, J.K. and von Blanckenburg, F.: Long-term stability of global erosion rates and weathering during late-Cenozoic
906 cooling. *Nature*: 465, 211-214, 2010.
- 907 Wittmann H., von Blanckenburg, F., Kruesmann, T., Norton, K.P. and Kubik, P.W.: Relation between rock uplift and
908 denudation from cosmogenic nuclides in river sediment in the Central Alps of Switzerland. *J. Geophys. Res.: Earth Surface*:
909 112 (F4), doi: 10.1029/2006JF000729, 2007.
- 910 Wittmann H., Von Blanckenburg, F., Guyot, J.L., Maurice, L., Kubik, P.W.: From source to sink: Preserving the cosmogenic
911 ^{10}Be -derived denudation rate signal of the Bolivian Andes in sediment of the Beni and Mamoré foreland basins. *EPSL*, 288,
912 463-474, doi: 10.1016/j.epsl.2009.10.008, 2009.
- 913
- 914
- 915